A STUDY OF THE INTERACTIONS OF MAGNETIC MATERIALS USING COUPLED FILMS WITH A CLOSED FLUX GEOMETRY

by

T. IWATA
J. S. SALLO

to

NATIONAL AERONAUTICS AND SPACE ADMINISTRATION
GEORGE C. MARSHALL SPACE FLIGHT CENTER
HUNTSVILLE, ALABAMA

Contract No.: NAS 8-20137

Period Covered: April 1965 to July 1966

August 2, 1966

A STUDY OF THE INTERACTIONS OF MAGNETIC MATERIALS USING COUPLED FILMS WITH A CLOSED FLUX GEOMETRY

by

T. IWATA
J. S. SALLO

to

NATIONAL AERONAUTICS AND SPACE ADMINISTRATION
GEORGE C. MARSHALL SPACE FLIGHT CENTER
HUNTSVILLE, ALABAMA

Contract No.: NAS 8-20137

Period Covered: April 1965 to July 1966

August 2, 1966

Presented by
Honeywell Inc.
CORPORATE RESEARCH CENTER
Hopkins, Minnesota

TABLE OF CONTENTS

		Page
I.	INTRODUCTION	1
II.	FUNDAMENTAL COUPLING MECHANISM STUDIES	2
	A. Vacuum System and Preparation of Coupled Films	2
	1. Vacuum system and experimental technique	2
	2. Preparation of films (Ni, Ni-NiO, Ni-Cu-Ni, Ni-Cu-Permalloy, and Cu-Permalloy	3
	B. Studies on Coupling Mechanism and Ripple Structure	7
	1. Magnetostatice interaction of ferromagnetic bodies separated by a non-magnetic layer (Studies on perpendicular anisotropy)	7
	2. Ripple structure caused by a rough non-magnetic layer in coupled films	9
	C. Creeping of Walls in Coupled Films	18
	1. Theory of wall creeping in thin films	18
	2. Stabilization of the Néel wall in coupled films	19
	D. Rotational Switching Threshold of Coupled Films	19
III.	COMPUTER ORIENTED MEMORY ELEMENT STUDIES	21
	A. Purpose of Study	21
	B. Deposition Facility	22
	C. Intermediate Layer	25
	D. Experimental Results	29
IV.	CONCLUSION	35

LIST OF ILLUSTRATIONS

Figure		Page
1	Electron Diffraction Patterns and Transmission Micrographs of Single Crystal Nickel Films	5
2	Cross Section of Film Types	11
3	Lorentz Electron Micrographs of a Ni-Cu Permalloy Film (Smooth Copper)	12
4	Lorentz Electron Micrographs of a Ni-Cu Permalloy Film (Rough Copper)	13
5	Lorentz Electron Micrographs of a Cu-Permalloy Film (Smooth Copper)	14
6	Lorentz Electron Micrographs of a Cu-Permalloy Film (Rough Copper)	15
7	Lorentz Electron Micrograph of a Cu-74% Ni-Fe Film (X500)	17
8	Block Diagram of Continuous Three Wire Plater	23
9	Processing of Three Wires Allowing Continuous Monitoring of Magnetic Characteristics of Individual and Coupled Film	24
10	Rate of Deposition of Paladium Chloride Immersion Coating	27
11	Rate of Deposition of Paladium Chloride Immersion Coating	28
12	Rate of Deposition of Electroless Copper Coating	30
13	Loops of Sample 94-1-E-4	33
14	Loops of Sample 94-1-E-5	34

		Page
APPENDIX 1 -	Perpendicular Anisotropy in Polycrystalline Ni-Fe Thin Films	1-1
APPENDIX 2 -	A Mechanism for Domain Wall Creeping in Magnetic Films	2-1
APPENDIX 3 -	Switching Characteristics of Uniaxial Ferromagnetic Thin Films with Superimposed Biaxial Anisotropy	3-1

I. INTRODUCTION

The objective of the work under contract No. NAS 8-20137 was to study the nature of coupling between ferromagnetic films separated by a non-ferromagnetic intermediate layer, in order to provide the basic knowledge for future designs of smaller high density more reliable magnetic memories. In order to accomplish these objectives we divided our efforts into two categories. The first was a fundamental study of the coupling mechanism, utilizing films prepared by vapor deposition techniques. This study was done primarily on single crystal films. The second portion of the program was a study of closed flux coupled film memory elements prepared by electro-deposition on copper wires. The combination of these two efforts has lead to a better understanding of the coupling mechanism as well as to a better insight into the eventual utility that coupled films may have in magnetic memory elements.

II. FUNDAMENTAL COUPLING MECHANISM STUDIES

A. VACUUM SYSTEM AND PREPARATION OF COUPLED FILMS

1. Vacuum System and Experimental Technique

In order to understand the mechanism of coupling between two ferromagnetic films separated by a non-magnetic layer, it is important to begin with single-crystal films formed by vacuum evaporation under controlled conditions. For the formation of these single-crystal thin films, an ultrahigh vacuum system along with accurate control of substrate temperature, residual gas pressure, and rate of evaporation, are necessary. Although no capital equipment was charged to the contract, it is appropriate to describe the equipment used in this study.

An ultrahigh vacuum system has been modified. This system utilizes a 100-liter/second Ultec ion pump capable of maintaining a vacuum of 10^{-9} Torr. Roughing is accomplished by a combination of mechanical and cryogenic pumps. The evaporation chamber is a belljar, 12 in. in diameter and 18 in. high. Using an appropriate vacuum collar; a Meissner liquid nitrogen trap, a mass-spectrometer gas analyzer (Aero Vac), a three-position electron beam evaporator (MRC), a film thickness monitor (Sloan), and a deposition rate controller (Sloan) have been installed. A vacuum of better than 3×10^{-7} Torr has been obtained with this system. The substrate holder and mask arrangement have been built capable of maintaining a 500° C temperature indefinitely.

Electron diffraction and transmission electron microscopy have been used to study the crystal orientation and grain size. The Lorentz method has been used to study domain nucleation and propagation as well as ripple structure. We were attempting to increase the magnification by Lorentz microscopy. In our previous work a magnification of 400X was achieved. We have now obtained magnification of up to 4000X.

An automatic torque magnetometer, which has been remodeled, and a conventional B-H loop tracer have been used for magnetic measurements.

2. Preparation of films (Ni, Ni-NiO, Ni-Cu-Ni, Ni-Cu-Permalloy, and Cu-Permalloy)

Using the vacuum system described above, multi-layer deposition was started with single-crystal Nickel films rather than alloy films. Nickel single-crystal films were deposited on sodium chloride single-crystal substrates so that the films could easily be removed by dissolving the substrate. Single-crystal nickel films, 600Å thick, were obtained by heat treating the substrate at 500°C for one hour prior to the deposition. The substrate temperature was maintained at 265°C and the pressure was held at less than 3×10^{-6} Torr during the evaporation. Electron diffraction analysis has proven these films to be very well oriented single crystals. In fact, there is no trace of a diffraction ring structure; the diffraction spots are sharp and discrete without streaking. However, satellite spots do appear about the strong nickel spots. These result from microtwins and double diffraction[1]. This has been proved by examining the satellite diffraction at different positions of the film. It was determined that the satellites vary in intensity and in some areas disappear completely. Upon further examination of the films, very weak diffraction shots are detected which may be due to impurities.

The mechanical buckling problem which we encountered in the early stages of the study was eliminated by lowering the substrate temperature during the pre-heat treatment. Further, we have studied the temperature of the substrate during the deposition. Finally films were deposited on substrates between 200° and 400°C. In all cases, single crystal films resulted. Post-deposition anneals were made as a means of eliminating the microtwins and buckling.

Some of the electron diffraction patterns of films produced at various substrate temperatures and annealed under different conditions are reproduced in Figure 1. Films annealed at 430° C for three hours show no signs of twinning, whereas films annealed at 370° still contained a large number of microtwins. Specimens annealed at 400° C for one to three hours have a very uniform structure and dislocations are easily observable. The dislocation density in our annealed specimen is quite low as compared to heavily cold-worked material. Domain walls have been observed on these nickel films. However, the domain walls cannot be propagated in the electron microscope with our present equipment because the coercive force is too high (about 5 to 100 oe).

The analysis of the single-crystal nickel on which we had attempted to grow single crystal nickel oxide epitaxially has been partly completed. Nickel oxide has been identified on the electron diffraction photograph.

Next, three-layer films have been grown. Initially a copper film and another nickel film were deposited on a single crystal nickel film. However, the films separated due to the poor adhesion of either the second or the third film. In order to eliminate the peeling, the first nickel layer was annealed and then the substrate temperature was reduced for the deposition of the copper and second nickel layer. By this method the three-layer films were formed. Electron diffraction patterns of three-layer film (Ni-Cu-Ni) show no evidence of a ring structure, indicating that there is no polycrystalline material present and that epitaxial growth continued through the top nickel layer. The diffraction pattern did show a few satellite spots indicating the presence of small amounts of microtwin formation, presumably in the upper unannealed layer. Domain walls have also been observed in this film and in one place it appears that we have seen the domain wall hung up on a dislocation; however, because of the high coercivity of the nickel film the domain wall could not be moved in the electron microscope.

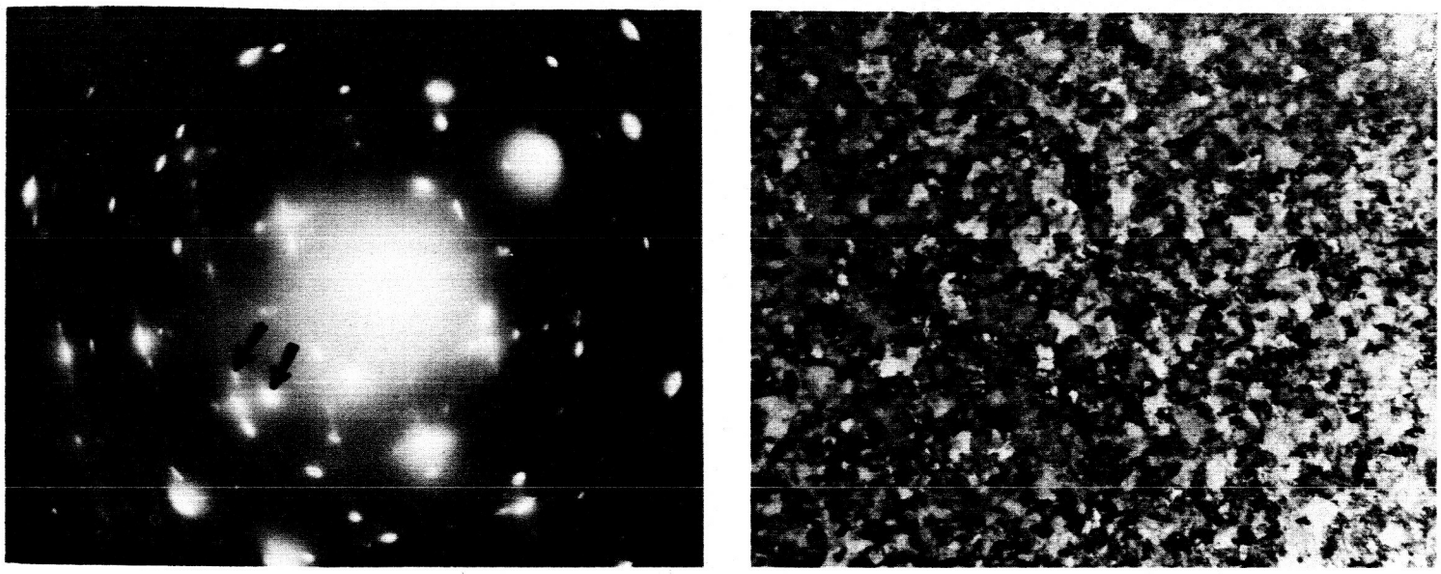

(a) (b)

Electron diffraction pattern (a) and transmission micrograph (b) of single crystal nickel film prepared at a substrate temperature of 175°C and annealed for 1 hour at 370°C. Arrows indicate satellite spots in diffraction pattern and twin planes in micrograph which give rise to satellite spots.

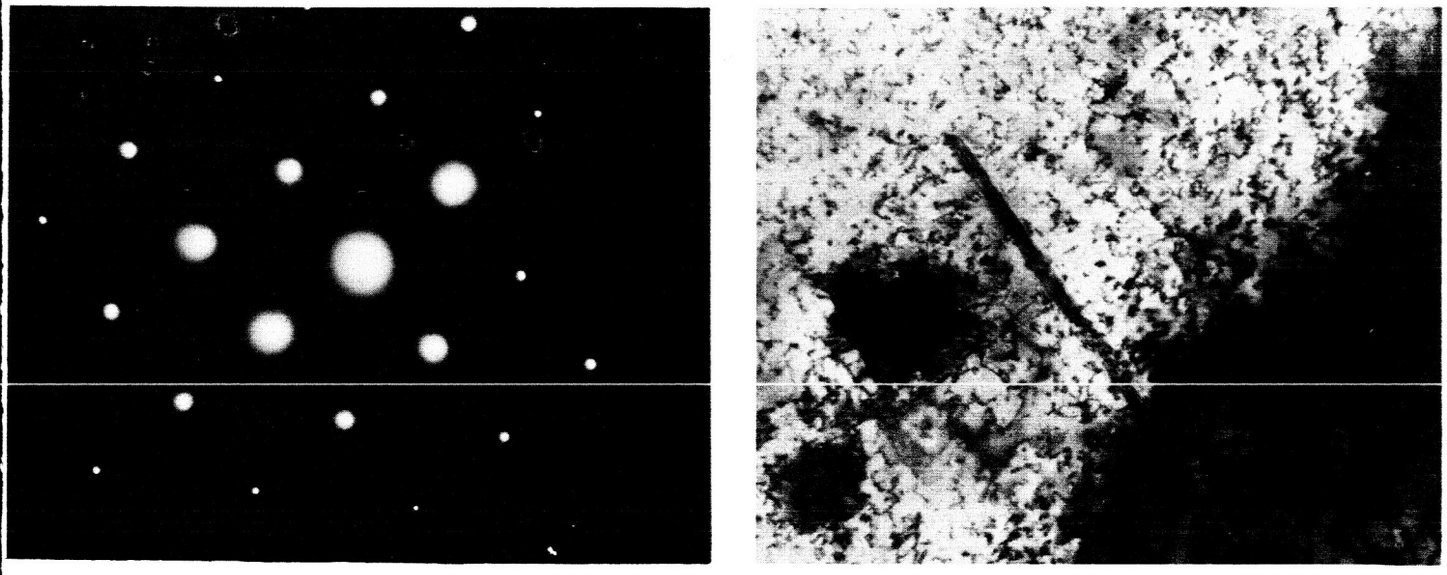

(c) (d)

Electron diffraction pattern (c) and transmission micrograph (d) of single crystal nickel film prepared at a substrate temperature of 215°C and annealed for 3 hours at 430°C. Note absence of satellite spots in diffraction pattern and absence of twin planes in micrograph. Diagonal band through center of picture shows dislocations caused by severely bending the film.

Figure 1 - ELECTION DIFFRACTION PATTERNS AND TRANSMISSION MICROGRAPHS OF SINGLE CRYSTAL NICKEL FILMS

Coupled films consisting of Ni-Cu-Permalloy have been prepared which have a coercive force of 10 – 14 oe. Domain walls have been observed on these Ni-Cu-Permalloy coupled films. These films were prepared by depositing the nickel film on a sodium chloride substrate at 200°C, followed by an anneal at 450°C for 1-1/2 hours. The subsequent copper and Permalloy layers were formed on a substrate held at room temperature and these were not subsequently annealed. The electron diffraction studies of these films showed a very well defined single-crystal pattern presumably of the first layer, nickel, and a superimposed ring pattern, presumably that of polycrystalline copper and Permalloy which were deposited at the low temperature. This indicates that subsequent single crystal layers deposited on a single-crystal film must be deposited at an elevated substrate temperature. The results of annealing samples at 2×10^{-7} Torr at 400°C for two hours has not been successful since the Permalloy remains polycrystalline or peels from the single crystal nickel layer.

Our attempts to form Cu-Permalloy single-crystal films have been quite successful. The Cu-Permalloy deposited on the sodium chloride substrate at 230°C appears to be a reasonably good single-crystal but much twinning still remains.

In these deposited single-crystal films, biaxial anisotropy is very dominant and little or no uniaxial character is evident.

B. STUDIES ON COUPLING MECHANISM AND RIPPLE STRUCTURE

1. Magnetostatic Interaction of Ferromagnetic Bodies Separated by a Non-magnetic Layer (Studies on Perpendicular Anisotropy)

In some previous work on magnetic thin films, we have shown that the crystallites of which a film is composed tend to grow in columnar form from the substrate[2]. A model was proposed (Prosen's model[2, 3]) which suggested that oxide forms preferentially along the grain boundary of these columnar crystallites. Recent experiments on perpendicular anisotropy[4, 5] tend to confirm this model, since the perpendicular anisotropy disappears if these films are formed under very high vacuum conditions, or if the partial pressure of oxygen is extremely low. By modifying Prosen's model so that sufficient oxide is formed on all sides of the column, thereby considerably reducing coupling from column to column, then, using the experimental results on columnar size[2], we can calculate a perpendicular anisotropy which very closely approximates that which is found in the experimental results[5]. It seemed that considerable progress in the understanding of the coupling mechanism could be made by further studying perpendicular anisotropy.

If Prosen's model is correct and the columnar cross-section is determined primarily by the substrate temperature, the perpendicular anisotropy constant ought to be a function of the columnar height or the film thickness. A series of polycrystalline Permalloy films of varying thickness have been formed on substrates at room temperature. These films were formed in a single evaporation with the residual gas pressure at 3×10^{-4} Torr. In these depositions, the thickness was varied from 100Å to over 3000Å. The perpendicular anisotropy has been found to be a function of the film thickness [c. f. Appendix 1, "Perpendicular Anisotropy in Polycrystalline Ni-Fe Thin Films", T. Iwata, R. J. Prosen, and B. E. Gran, J. Appl. Phys. 37, 1285 (1966); this paper was originally presented at the Conference

on Magnetism and Magnetic Materials, San Francisco, November, 1965]. Previous work had shown the perpendicular anisotropy to be a function of alloy composition and substrate temperature[5].

Four possible models for the explanation of this perpendicular anisotropy have been considered:

i) Magnetostatic model - The magnetostatic model is essentially Prosen's model[2, 3] in which the film is composed of crystallites which grow in columnar form from the substrate. The coupling from column to column is substantially reduced or eliminated by the presence of impurities or oxides along these grain boundaries. This magnetostatic model would not only account for the dependence of perpendicular anisotropy upon the composition and substrate temperature, but also is expected to have a thickness dependence such as we have found experimentally.

ii) Surface anisotropy model - In this model, we have not only considered the surface anisotropy[6] which is obtained from the overall film surface, but also the surface anisotropy which would result by assuming a columnar growth in which the columns are essentially independent and have their own surface anisotropy. According to this model, we would anticipate no thickness dependence of the perpendicular anisotropy.

iii) Exchange anisotropy[7] model - This model would include the effect of an antiferromagnetic surface layer of oxides as well as the effect of an antiferromagnetic phase along the grain boundaries of the columnar growth. Since the possible antiferromagnetic phase is nickel oxide, one might reasonably expect a different compositional dependence (i.e., decreasing with increasing iron content) from that which was obtained[5].

iv) Stress model - The stress model, likewise, has two considerations: the isotropic stress within the entire film due to the difference in expansion coefficients between the substrate and the film, as well as anisotropic stress originating within the columnar structure due to preferential oxidation. For this model one would expect the variation in perpendicular anisotropy to approximate the magnetostriction curve for the varying alloy compositions.

It appears that the magnetostatic model is best able to account for all the experimental work to date. Details of this model are given in Appendix 1.

Interesting papers related to this model have recently been published. Wade and Silcox[8] have reported small-angle electron diffraction observation of the columnar structure in several films including Permalloy films. The results of the magnetic measurements newly obtained by some researchers[9, 10] all support our model and, further, Fujiwara[11] has proposed a model which is essentially the same as ours.

2. Ripple Structure Caused by a Rough Non-magnetic Layer in Coupled Films

There may be many possibilities for causing the domain walls to stick in coupled films. This gives rise to an improvement in the wall-creeping characteristics of the thin film. Wall-wall interaction in coupled films is an already proposed mechanism for reducing wall-creeping[12].

Variations in the thickness of the intermediate non-magnetic layer will provide locations where the domain walls can stick. Such locations also can lead to local fluctuations of the direction of magnetization caused by stray fields. Therefore a close relationship is expected between the ripple structure and wall-creeping. Thus, our initial study has concentrated on an investigation of the ripple structure in coupled films with a periodic variation of the intermediate non-magnetic layer.

Four types of films have been formed (Figure 2) which we expect will exemplify the effect of variations in the coupling layer thickness as well as the effect of a periodic variation in the substrate roughness. The first type of film (Figure 2-a) includes a 400Å single-crystal nickel film formed on a sodium chloride substrate, a second layer of copper about 100Å thick and a third layer of polycrystalline Permalloy 400Å thick. The second type of film (Figure 2-b) is similar to this structure except that the continuous copper film is 50Å thick and has superimposed on it a series of 50Å thick, 30μ wide mounds which are located on 50μ centers. The third and fourth types of films are identical to the first and second except that the initial nickel layer has been eliminated (Figure 2-c and 2-d). In forming these last two types, we were much more successful in obtaining single crystal Permalloy films. The Lorentz patterns for these four cases are quite different.

Figures 3 through 6 show the Lorentz electron photographs of these four types of films under various applied fields. It is striking to note that the ripple structure as seen in Figure 3, corresponding to Figure 2-a, has the least amount of ripple and corresponds to the usual type of ripple seen in ordinary Permalloy films[13]. On the other hand, Figure 5, which corresponds to the structure as depicted in Figure 2-c, has considerably more ripple structure. We attribute this difference to the fact that the 100Å copper layer growing on top of a nickel film will be more continuous and have less island characteristics than when it grows on a sodium chloride substrate. The island structure of the copper layer will cause free poles to form in the superimposed, continuous Permalloy film. The magnetostatic energy of these free poles will tend to increase the ripple structure just as the free poles of pinholes and occlusions markedly affect the magnetization ripple in Permalloy films. In Figure 6, which corresponds to Figure 2-d, the ripple pattern is further enhanced. In addition, the ripple pattern follows the island nature of the copper layer. Finally, in Figure 4, which corresponds to Figure 2-b, actual domains are seen, even in the zero field state, corresponding to the periodic roughness

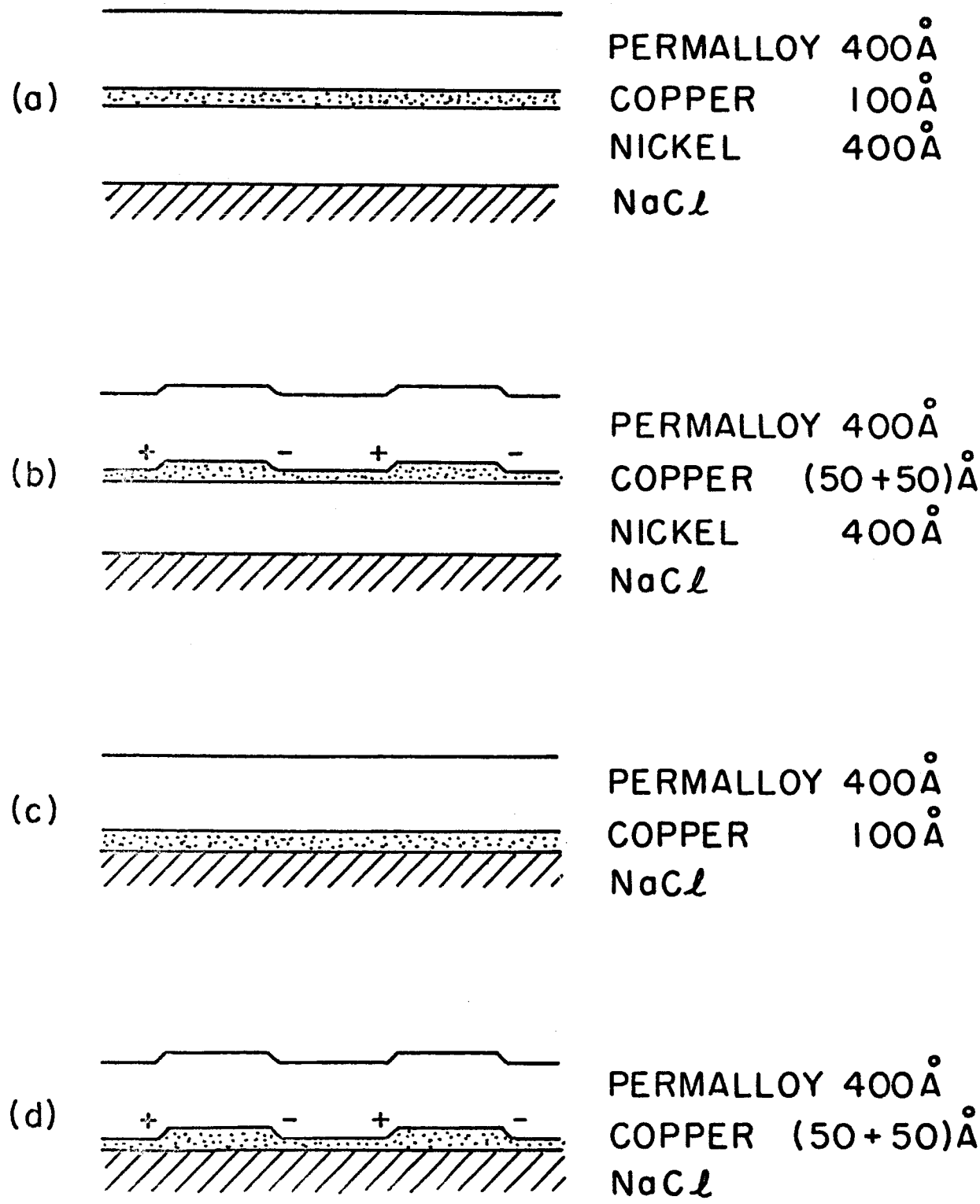

Figure 2 - CROSS SECTION OF FILM TYPES

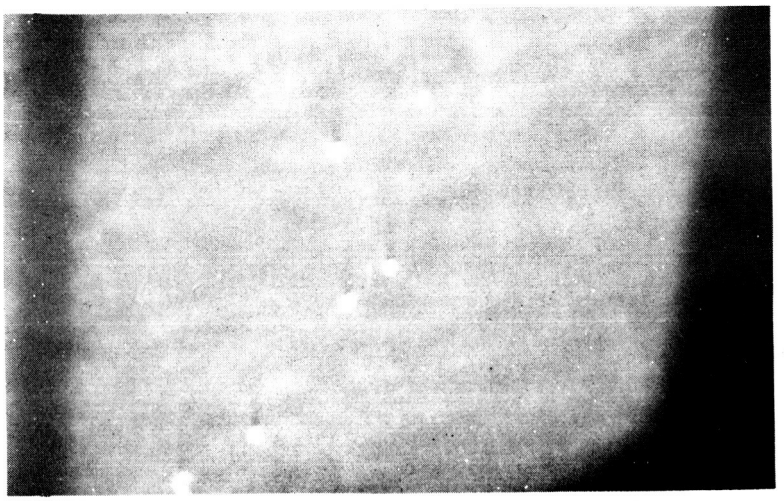

1433-34 5.1 oe

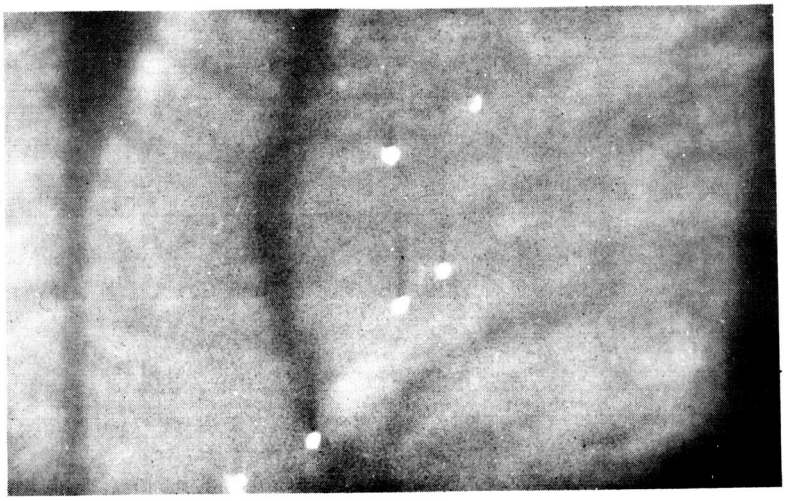

1433-35 6.8 oe

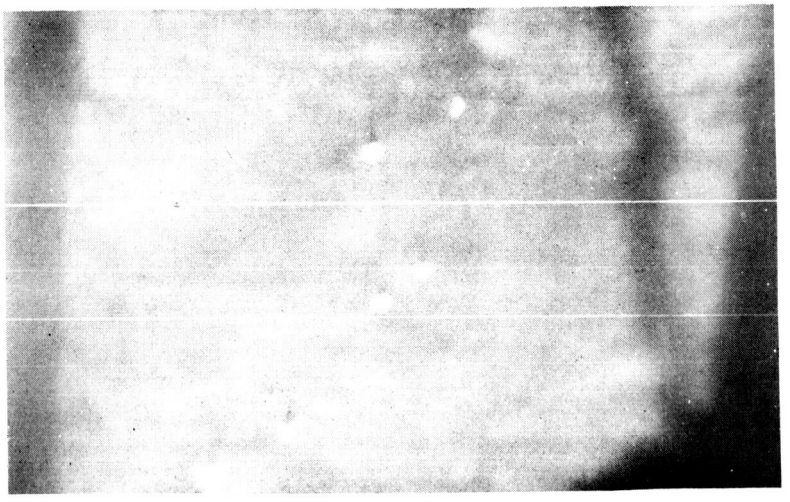

1433-36 8.5 oe

Figure 3 - LORENTZ ELECTRON MICROGRAPHS OF A Ni-Cu PERMALLOY FILM (SMOOTH COPPER)

1433-31

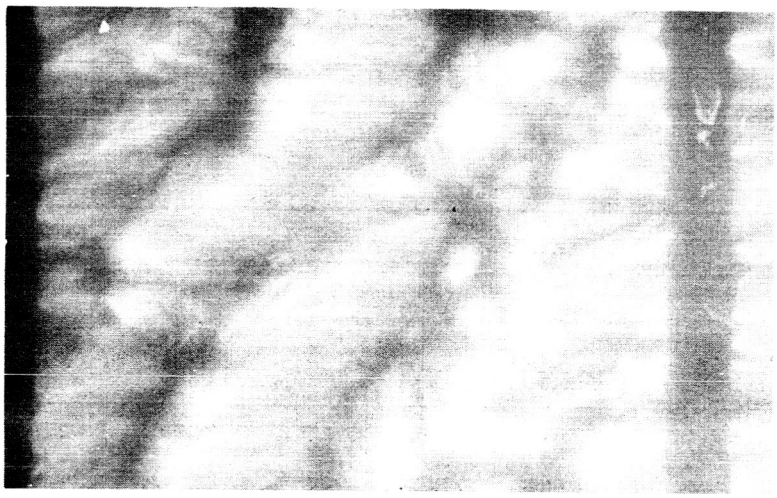

7.6 oe

1433-32

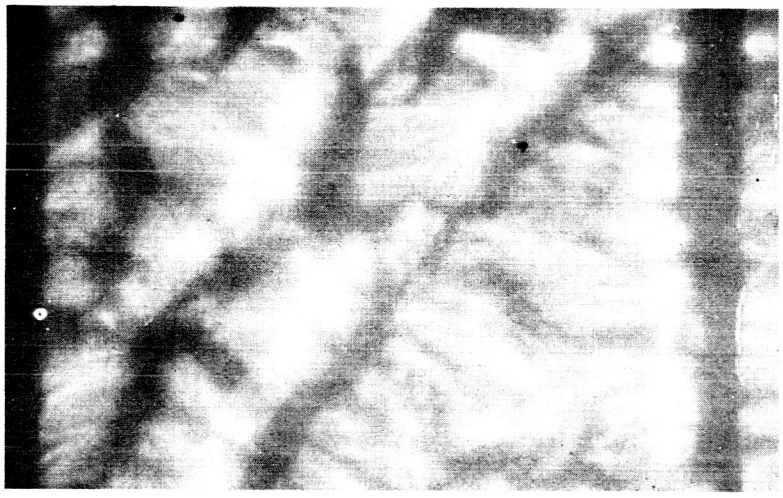

9.3 oe

1433-33

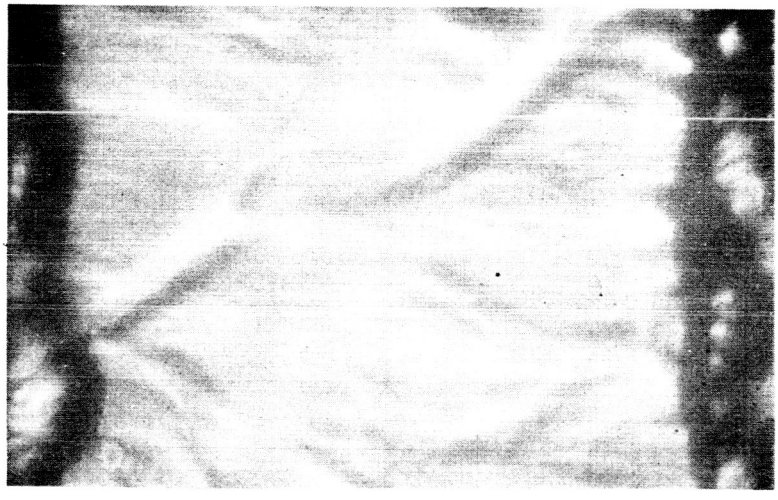

13.6 oe

Figure 4 - LORENTZ ELECTRON MICROGRAPHS OF A Ni-Cu PERMALLOY FILM (ROUGH COPPER)

1433-16

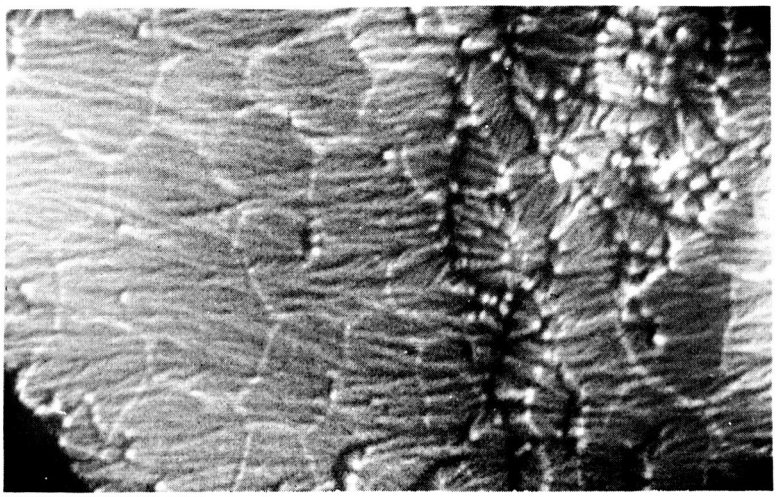

No Field

1433-17

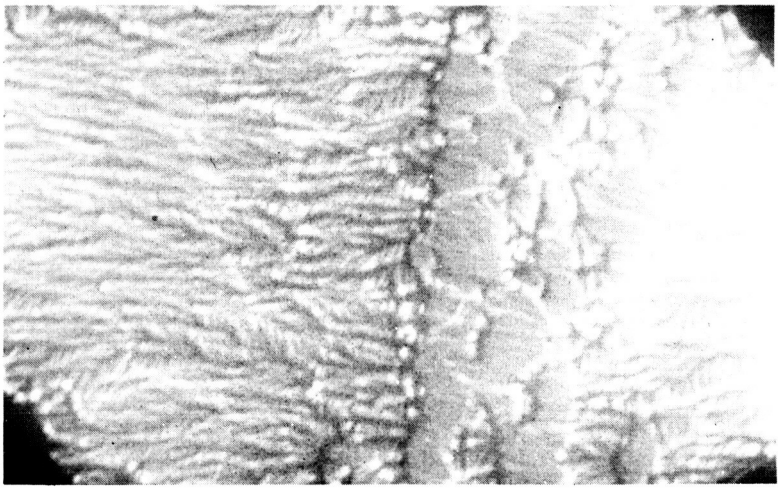

+15 oe

1433-18

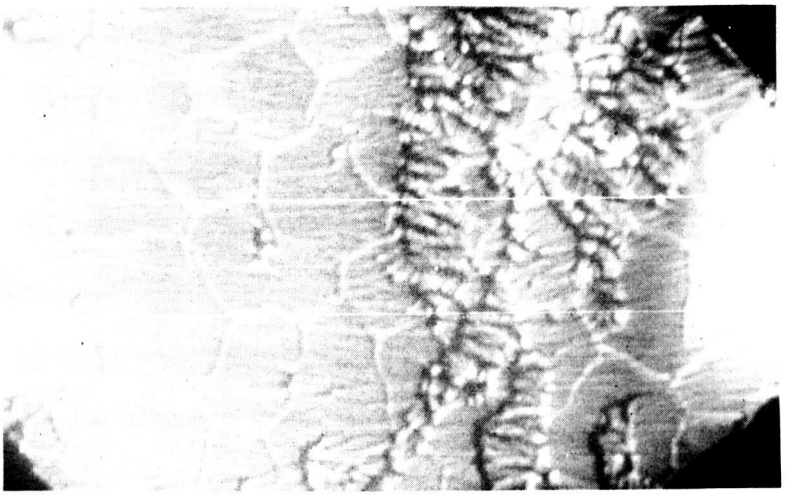

- 15 oe

Figure 5 - LORENTZ ELECTRON MICROGRAPHS OF A Cu-PERMALLOY FILM (SMOOTH COPPER)

1433-10

No Field

1433-11

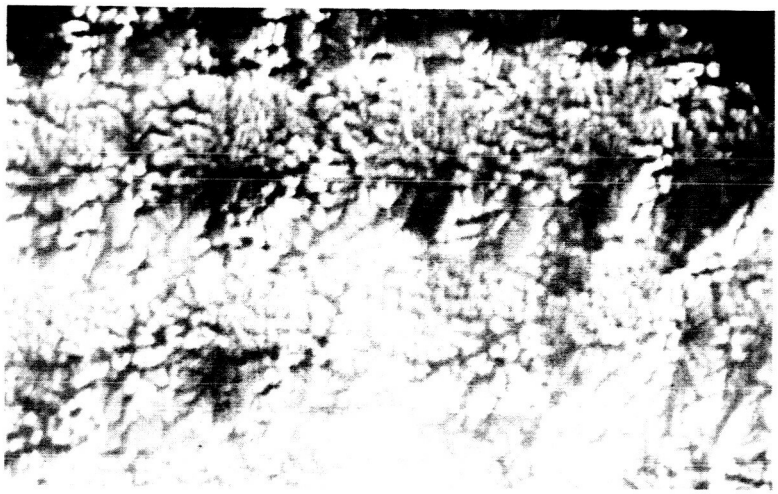

+15 oe

1433-12

- 15 oe

Figure 6 - LORENTZ ELECTRON MICROGRAPHS OF A Cu-PERMALLOY FILM (ROUGH COPPER)

of the copper layer. The close proximity of the black and white line can be interpreted as a 360° wall. The two 180° portions of this wall tend to hang up on the free poles formed as a result of the copper thickness variation. Upon application of a field along one of the easy directions, the 360° wall separates to form actual domains with the two 180° walls separating. Again, the 180° walls tend to hang up on the free pole areas, i.e., along the rows or columns of the copper islands.

From the results of this experiment, it has been suggested that the island characteristics of thin copper layers will cause free poles in the superimposed continuous Permalloy film and that the stray fields from these free poles increase the ripple structure. To further confirm this, the following experiment has been conducted. The usually accepted cause[13] of ripple is a magneto-crystalline anisotropy fluctuation due to random distribution of crystallites. In order to avoid this ripple structure, assuming this theory to be correct, layered films, similar to Figure 2-c and composed of an initial copper layer and a subsequent zero magnetocrystalline anisotropy Ni-Fe (74% Ni), have been deposited onto newly cleaved NaCl surfaces. During the deposition the substrate temperature was held at room temperature and a magnetic field was applied in the plane of the film. Selected area electron diffraction patterns indicate a random orientation of crystallites in the films. The mean diameter of the crystallites is of the order of 100Å. A typical film (100Å Cu and 1000Å Ni-Fe) has a coercive force of 3 oe and an anisotropy field of 5 oe.

The Lorentz electron micrographs of this film indicate the presence of magnetization ripple (Figure 7). If the origin of the ripple is only in the randomly oriented magneto-crystalline anisotropy, the absence of magnetization ripple is to be expected for zero magneto-crystalline anisotropy films. Therefore, although extensive studies are necessary to arrive at a definite conclusion, the observed ripple seems to be attributable to the free poles created by the island characteristics of the thin copper layer.

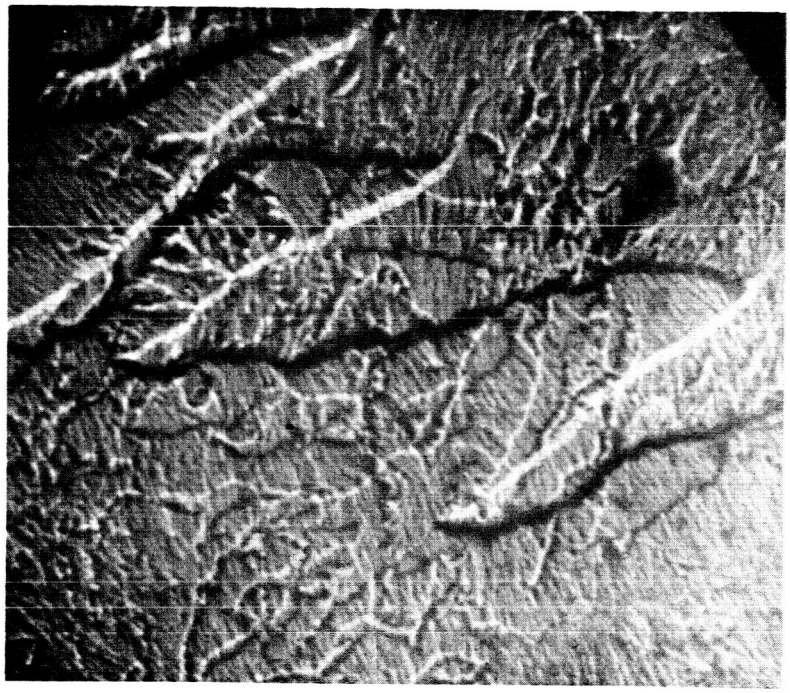

Figure 7 - LORENTZ ELECTRON MICROGRAPH OF A Cu-74% Ni-Fe FILM (X500)

Since the wall coercive force, creeping of walls, etc., are affected by ripple structure, structural aspects of the intermediate non-magnetic layer will be an important factor in the magnetic characteristics of coupled films.

The studies described in this chapter (B.2.) will be submitted for publication to the Conference on Magnetism and Magnetic Materials to be held in November, 1966 at Washington D.C.

C. CREEPING OF WALLS IN COUPLED FILMS

1. Theory of Wall Creeping in Thin Films

Minimizing wall-creeping is an important problem in thin film application. However, at present, the cause of wall-creeping even in the single film is quite unclear[14]. In this section, this subject will be considered.

A uniaxial thin film composed of magnetic domains separated by parallel walls (Néel or Bloch wall) has been considered. The anisotropy energy and magnetic energy of domains and the wall energy as well as the magnetostatic energy of the whole system have been taken into account. Because of the large free pole energy inherent in the Néel wall, even in the absence of an applied field, the magnetizations of neighboring domains separated by the Néel wall deviate from their easy axis and make an angle with one another which is slightly different from 180°. When magnetic fields are applied, this domain-magnetization canting gives rise to an additional pressure on the wall, and therefore wall creeping is induced in some cases. For Bloch walls, such canting does not occur and no appricable creep is expected. Calculated threshold curves combined with the irreversible Bloch-line motion in Néel walls could account for the main features of wall creeping. Details of the theory is given in Appendix 2 [A Mechanism for Domain-Wall Creeping in Magnetic Films, T. Iwata, to be submitted for publication.]

2. Stabilization of the Néel Wall in Coupled Films

In a three-layer film consisting of two magnetic layers separated by a thin non-magnetic layer, the stray field created by the free poles in the wall in one layer will cause the magnetization in a region above the wall in the second layer to rotate in a direction anti-parallel to the magnetization in the wall. Thus the Néel wall in one layer is easily accompanied by a Néel wall or a quasi-Néel wall in another layer[12, 15]; the wall in the second layer acting as a keeper for the flux of the Néel wall in the first layer. Stray fields in the domains at both sides of the Néel wall are reduced substantially by this effect and domain-magnetization canting is eliminated. Therefore, based on the theory discussed in the previous chapter (C. 1.), it can be said that the Néel walls in coupled films can be stabilized against creeping. This may be an explanation of the experimental result that the amount of wall-creeping is reduced substantially in coupled films[12].

D. ROTATIONAL SWITCHING THRESHOLD OF COUPLED FILMS

So far the discussions have been made on the intrinsic magnetic properties of thin films such as anisotropy and ripple structure as well as on the aspect concerning wall motion. Now, we will discuss the rotational switching of coupled films. Consideration has been given to the role of anisotropy on the switching threshold. In general, each component layer of a coupled film can have its own magnetic anisotropy, and these can differ in symmetry. One of the simplest cases is that in which one of two strongly coupled layers has uniaxial anisotropy while the other layer has biaxial anisotropy and the biaxial easy axis makes an angle of 45° with the uniaxial easy axis. Calculations of rotational switching threshold curves and B-H loops for typical cases are given in Appendix 3 [Switching Characteristics of Uniaxial Ferromagnetic Thin Films with Superimposed Biaxial Anisotropy, T. Iwata, to be submitted for publication]. In some cases, calculated switching

curves deviate remarkably from the uniaxial switching asteroid originally given by Stoner and Wohlfarth[16], and it has been indicated that some of these types of coupled film should display favorable NDRO switching characteristics.

The calculation has been made only for the case of two strongly coupled layers (or of a single layer which possesses two anisotropies). If the coupling is so weak or the two layers are so thick that incoherent rotation occurs in the direction perpendicular to the film plane, the NDRO property derived above may be modified. Many possibilities for NDRO application can be expected from the controlled preparation of coupled films.

III. COMPUTER ORIENTED MEMORY ELEMENT STUDY

A. PURPOSE OF STUDY

Plated wire memory elements appear to have a number of advantages making them ideally suited for high speed random access computer memory applications. Among these advantages are high-speed, high-signal outputs relative to flat thin films, and relative ease of obtaining non-destructive readout operation. A number of memory systems utilizing plated wire have been described and a number of further applications for plated wire are presently being investigated. The main disadvantage of these plated wire elements appears to be a sensitivity to creep. Creep appears to be a more serious problem in these elements than in flat magnetic thin films. This is so because the plated wire elements are usually plated to a greater thickness than are flat thin films, and because the plated wire element utilizes a continuous magnetic material. The greater thickness of plated wire elements is responsible for the advantage of higher signal output and is possible because of the closed flux geometry and the lack of demagnetizing effects. The continuous nature of the magnetic medium is due to the continuous electrodeposition which is used as a means of producing wire elements in an economical fashion. One way of eliminating the creep problem in plated wire elements is to use a dual phase write system so that the element never sees more than two consecutive pulses of the same polarity. Although this electrical technique is successful it has the disadvantage of slowing down the write cycle time and of requiring close tolerances on the positive and negative digit pulses which are used.

Recent publications have shown that creep should theoretically be diminished in flat films through the use of coupled films[12]. Additional work has been done by certain groups in an attempt to provide an experimental verification of these theories.[17, 18] It is, therefore, to be expected that, in plated wire

and flat film elements, coupled films will provide an improvement in the problem of domain-wall creeping. If this is the case, a greatly improved plated wire memory element could be obtained through the utilization of coupled film techniques. For this reason this portion of the contract was initiated to determine whether or not coupled plated wire elements could be fabricated and to obtain preliminary data on the magnetic properties which could be expected from such elements.

In order to achieve the advantages which might result from the coupled film geometry, it is necessary to have films of differing H_k. As a result of other programs in plated wire elements, Nickel-Iron films having various values of H_k were made available for this study. The particular films chosen had an H_k of approximately 1.8 oersteds and 2.9 oersteds respectively.

B. DEPOSITION FACILITY

In order to determine the properties of the coupled films and the effect of the coupling mechanism itself, it is necessary to have carefully controlled conditions for the development of the two magnetic coatings and the coupled structure. In order to best provide this, a three-wire plater was constructed. Figure 8 shows a drawing of the essential features of this plater, and Figure 9 shows a photograph of the finished plater. Utilizing this plater, it was possible to plate three wires simultaneously and to test them on line immediately after this plating. Therefore, through the use of this plater it was possible to study each layer separately as produced on two of the lines, and the coupled layer as produced on the third line. In this way all three layers could be produced at the same time from the same solutions and could be directly compared. This plater was used to prepare the first coupled wires that were made in this program.

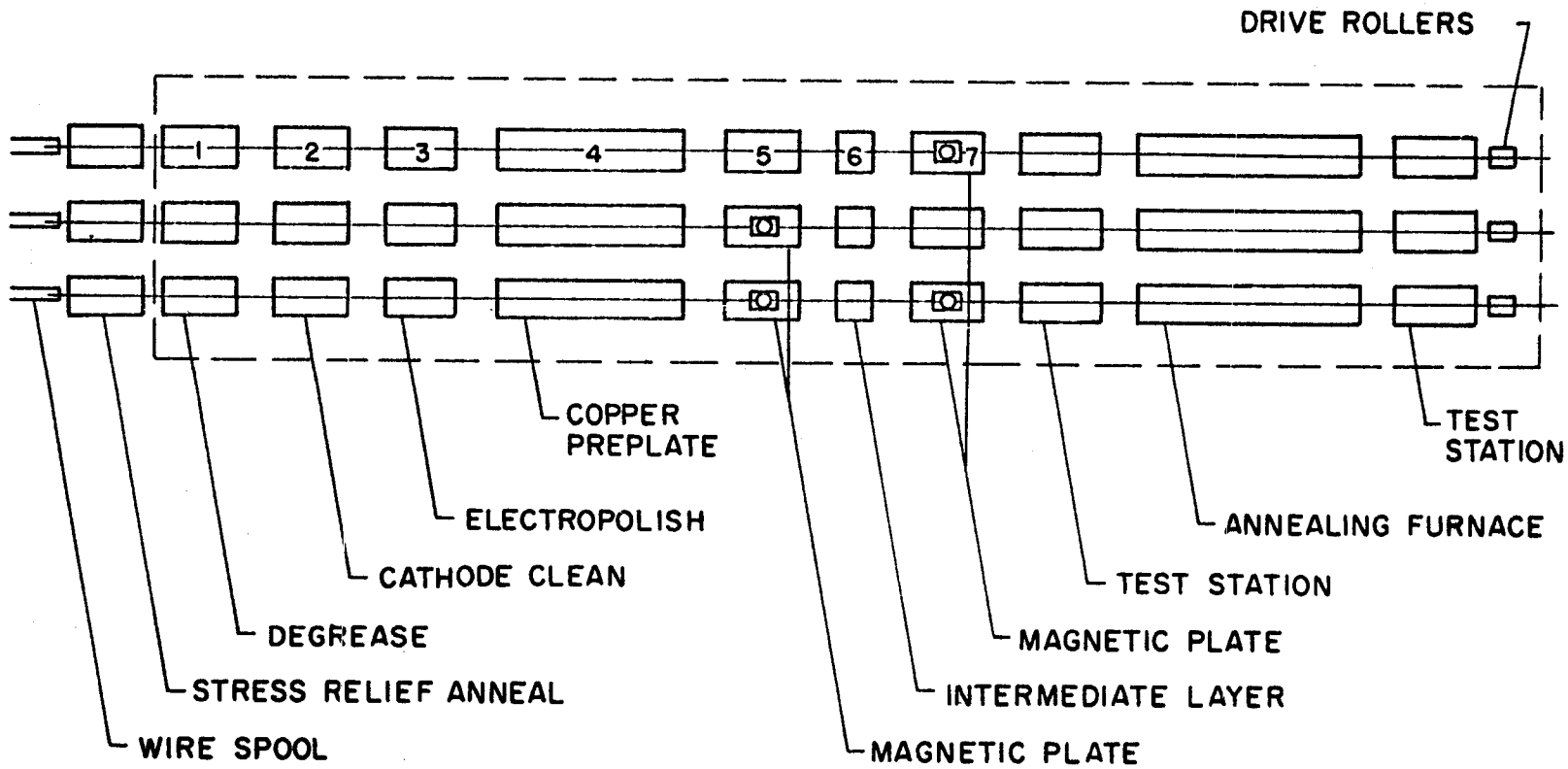

Figure 8 - BLOCK DIAGRAM OF CONTINUOUS THREE WIRE PLATER

Figure 9 - PROCESSING OF THREE WIRES ALLOWING CONTINUOUS MONITORING OF MAGNETIC CHARACTERISTICS OF INDIVIDUAL AND COUPLED FILM

As the program developed one of the major problems with the plated wire elements was that of skew. Careful studies on other programs indicated that this skew was due primarily to a twist in the substrate wire during deposition. It was found that the best way of preventing this twist was to push the wire through the plater. Further studies showed that the three-wire plater utilized in this program, due to its length, would be difficult to modify so that the wire could be pushed through the plater. It was decided to utilize another plater for the production for the last batches of plated coupled film wires.

In order to know the parameters of each of the plating cells, the following technique was used: The plating was done from three successive plating stations as shown in Figure 8 for the three-wire plater but utilizing only one line. The properties of the first plate were investigated by turning off the current in the second and third platings and the properties in the third plate were investigated by turning off the current in the first and second platings. Although this was not quite as satisfactory a control as was available through the use of the three wire-plater it did turn out to be adequate for our purposes. The original three wire plater, although still available and functional, has, therefore, not been modified so that the wire can be pushed through the plating cells.

C. INTERMEDIATE LAYER

Several studies have shown that very thin non-magnetic metallic layers should be used as the intermediate layer in these coupled films. When one considers the geometry and the mechanical problems in the wire plating operation it becomes clear that only two techniques are available for depositing this layer: electro-deposition and electroless deposition. Electro-deposition is capable of yielding very thin deposits; however, the thickness of the deposits must be controlled by a very careful and accurate control of the current which

is applied during deposition and will also be dependent upon the cathode efficiency of the plating operation. Although control of plating thickness will be difficult utilizing this technique, it is possible that it could be achieved with a wide variety of non-magnetic materials.

Another possible way of solving this problem is to use an immersion or electroless plating which plates at a much slower plating rate than most electro-deposition processes and therefore, should be more readily controlled at very low thickness. In addition, these electroless deposits are in general insensitive to geometry effects and very thin uniform coating should be readily obtainable. It was decided to investigate this electroless approach for both palladium and copper in the hopes that it would prove superior to electro-deposition for depositing the intermediate non-magnetic metallic layer.

In order to utilize these electroless coatings it is necessary to know to a great degree of accuracy the thickness of coating which will be produced within a given plating time. In order to determine these deposition rates, radioactive tracer techniques were utilized and radioactive Pd and Cu were added to the electroless Pd and Cu baths respectively. Figure 10 shows the results obtained from the immersion Pd coating when the deposit was formed at a pH of 1.2 and$PdCl_2$ concentration of 1.25 milligrams per ml on both the plated wire or nickel-iron substrate and the copper wire substrate. Figure 11 shows similar results at a pH of 2.1 at $PdCl_2$ concentration of 0.5 mg/ml. Other combinations of variables were also investigated.

Since the deposit will be formed on the nickel-iron substrate, these curves are of greater significance than are the curves on the copper substrate. It appears from these curves that if very thin deposits are to be achieved, extremely short times will be required. This means, since the rate of movement of the wire through the balance of the plating system is fixed, that extremely short plating cells will be required. In addition, it was found that the $PdCl_2$ plating bath has a detrimental effect upon the magnetic properties

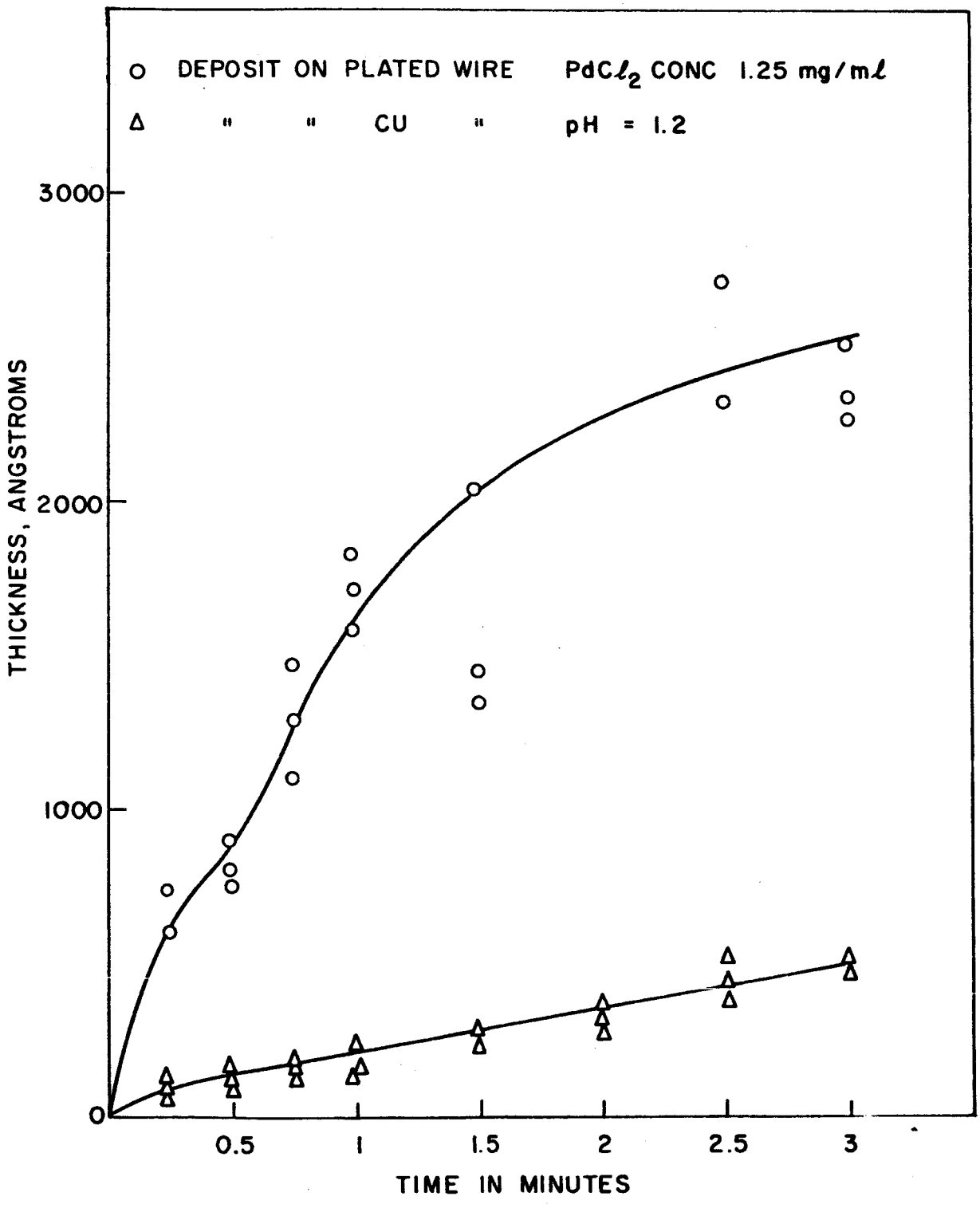

Figure 10 - RATE OF DEPOSITION OF PALADIUM CHLORIDE IMMERSION COATING

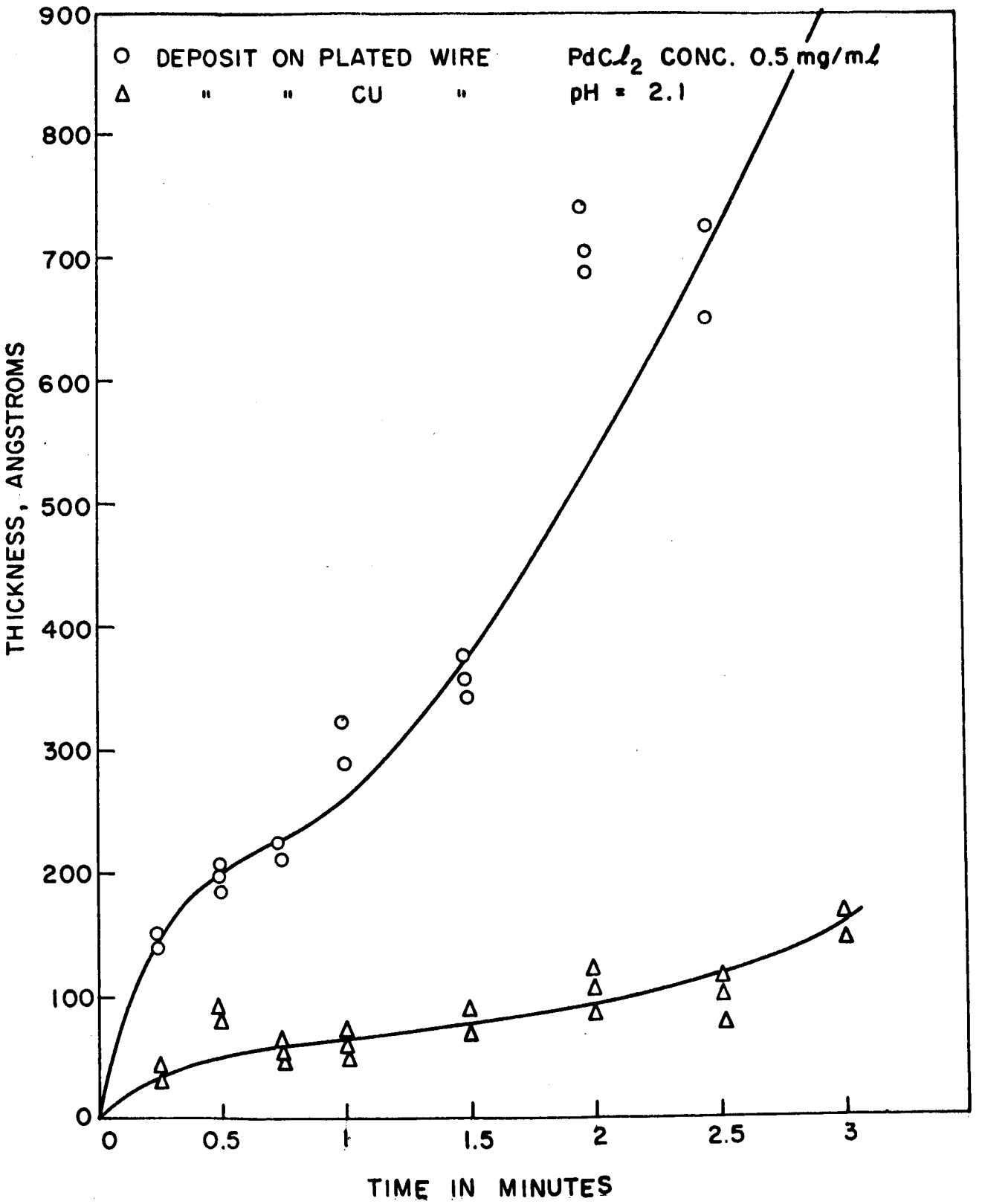

Figure 11 - RATE OF DEPOSITION OF PALADIUM CHLORIDE IMMERSION COATING

of the magnetic layer which is laid down prior to the Pd deposit. This was shown to be a consequence of the low pH required in this system. These two disadvantages would seem to rule out the use of this particular plating system as the intermediate layer in the coupled structure.

Figure 12 shows similar data obtained by adding radioactive Cu to a Shipley proprietary copper bath. Although this deposit has no adverse effect upon the magnetic coating it is clear that in the very thin region exceedingly small plating cells will be required due to the very short time which must be utilized. On the other hand, coatings on the order of 600 Å could be readily achieved from this system. As a result of these studies it was determined to attempt to electro-deposit copper as the first intermediate layer of the coupled structure since its thickness could be more readily controlled in a plating cell of more conventional size. A copper pyrophosphate bath was modified by dilution and used at very low current density in order to achieve this thin copper deposition. In addition a very precise control of plating current was added to the system so that currents in the microampere range could be used.

D. EXPERIMENTAL RESULTS

Under the conditions of the deposition, each Ni-Fe layer has a thickness of 3000Å. In all cases two magnetic layers are present so that the aggregate magnetic material has a total thickness of 6000Å. If a copper layer is present, it occurs between the 3000Å permalloy films. The thickness of the copper layer is not known. Its maximum average thickness was calculated assuming 100% cathode efficiency and uniform thickness of the deposit. All samples were at or near zero magnetostriction. Until the copper layer reached a thickness of 320Å the combined film showed a single coercive force, a behavior similar to that reported previously[19]. Values of H_k and H_c for a series of deposits of varying copper thickness are shown in

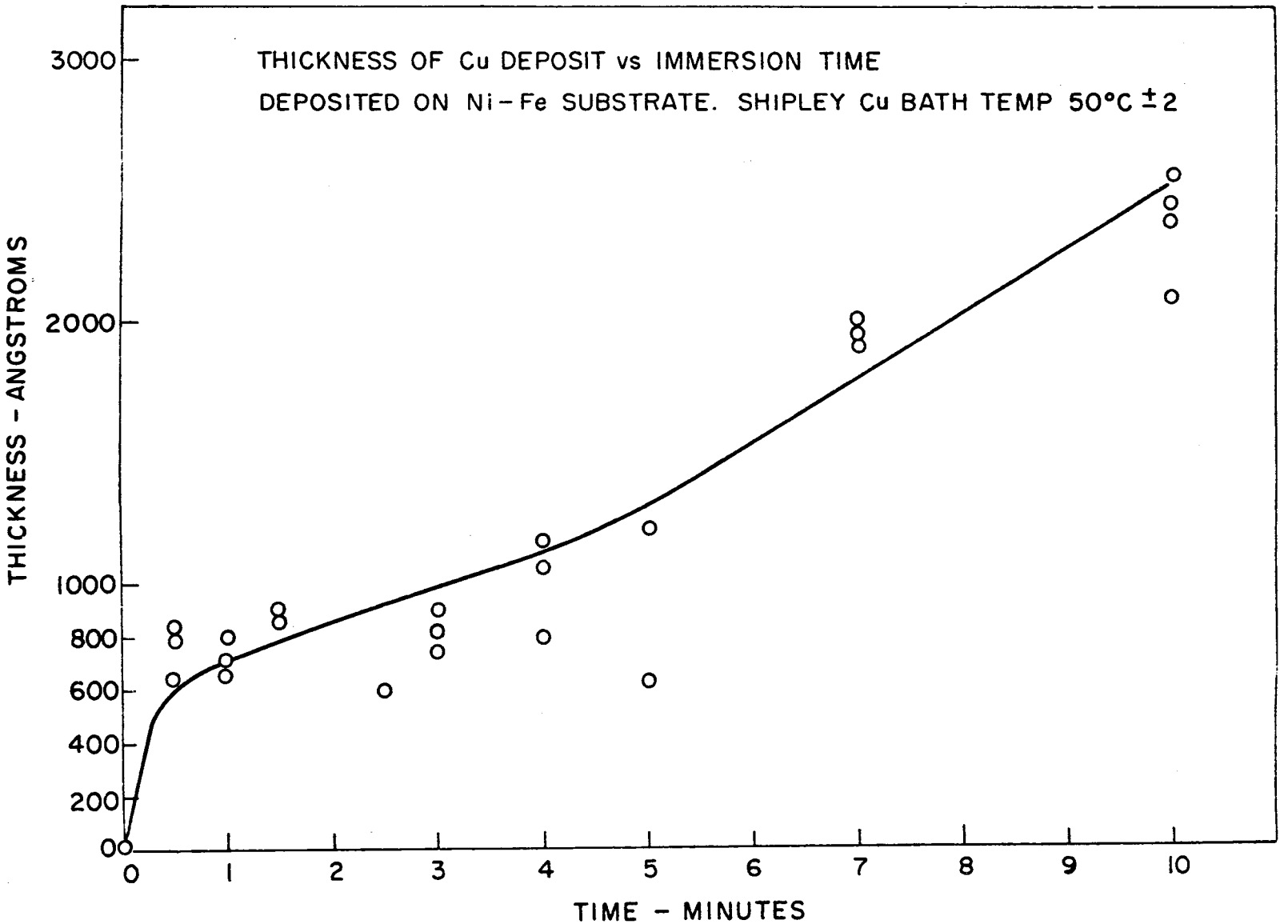

Figure 12 - RATE OF DEPOSITION OF ELECTROLESS COPPER COATING

Table I utilizing the calculated maximum value for copper thickness. The deposit type refers to the type (high H_k or low H_k) formed from each of the two deposition cells.

Table I shows no appreciable variation of H_c as a result of the coupling. The H_k variation appears to be real. The initial coupled film with no copper intermediate (A-B) assumes the H_k of the lower H_k single film (A-A). The very thin copper layer causes no change, perhaps indicating a discontinuous copper layer. The decrease in H_k at 80Å of copper appears to be real although no explanation can be offered. Further increase in the copper thickness leads to a gradual increase in H_k until the sandwich has H_k greater than either film A or B alone. At very high copper thickness (i.e., 2400Å) H_k is very low. This behavior of H_k cannot be explained at the present time.

Figure 13 shows the unintegrated easy and hard direction hysteresis loops of sample 94-1-E-4. Stepped loops first appeared in sample 94-1-E-5 (Figure 14).

Pulse tests on these elements were not conclusive. Several of the samples show NDRO properties, but none are improvements over sample 91-1-E which is not coupled. Preliminary creep and adjacent bit interference studies were not conclusive.

The unusual H_k effects and the stepped loop appearance require further study. The appearance of NDRO properties makes these coupled structures worthy of further device studies.

TABLE I

H_k AND H_c VALUES FOR DEPOSITS OF VARYING COPPER THICKNESSES

Sample	Type	Copper	H_k	H_c
92-2-E	A-A	0	1.8 oe	2.7 oe
91-1-E	B-B	0	2.9	3.0
92-1-E	A-B	0	1.9	3.0
94-1-E-1	A-B	30Å	1.7	2.6
94-1-E-2	A-B	80A	1.3	3.2
94-1-E-3	A-B	160	2.2	2.5
94-1-E-4	A-B	240	3.1	2.5
94-1-E-5	A-B	320	2.4	3.0
94-1-E-6	A-B	400	2.9	2.8
94-1-E-7	A-B	480	3.6	3.1
94-1-E-8	A-B	560	3.6	2.8

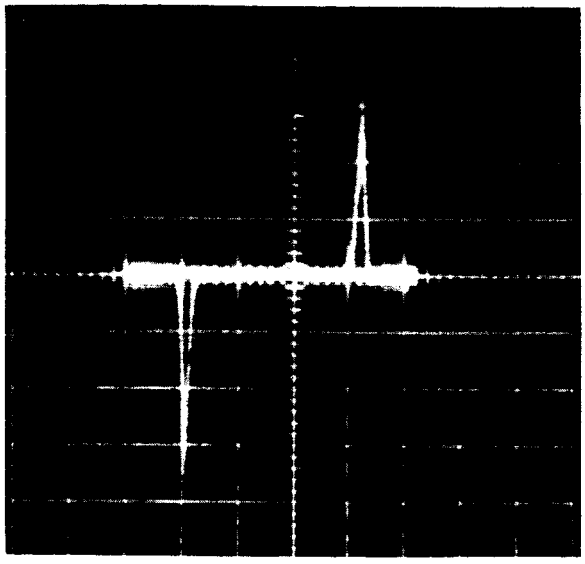

EASY DIRECTION LOOP

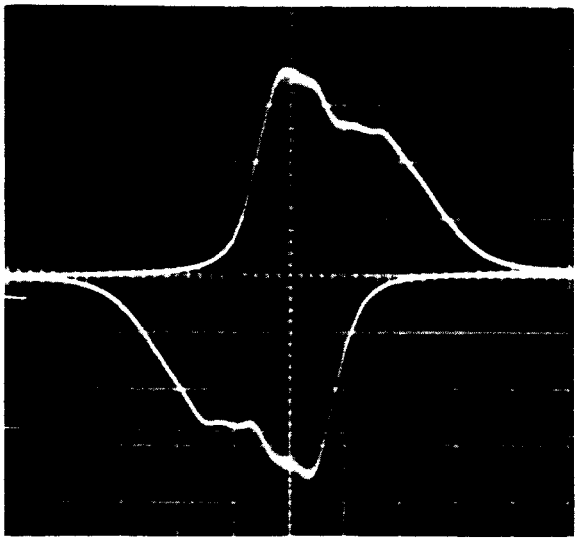

HARD DIRECTION LOOP

Figure 13 - LOOPS OF SAMPLE 94-1-E-4

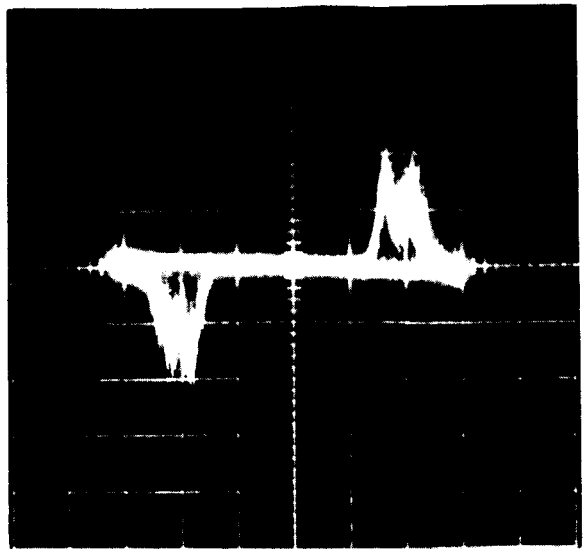

EASY DIRECTION LOOP

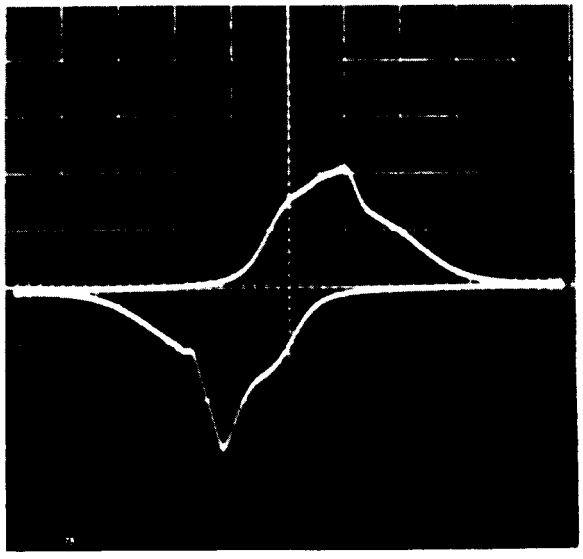

HARD DIRECTION LOOP

Figure 14 - LOOPS OF SAMPLE 94-1-E-5

IV. CONCLUSIONS

Our studies in perpendicular anisotropy have already been published and appear as Appendix 1 of this document. It has been shown that the free-pole energy associated with columns of ferromagnetic material growing perpendicular to the substrate is responsible for the perpendicular anisotropy. These studies not only lend support to our previously proposed model for the occurrence of uniaxial anisotropy in evaporated ferromagnetic film but also provide the starting point for the following experiments.

The concept of utilizing a variable thickness intermediate layer to cause sticking of domain-walls and thereby reduced domain-wall creeping in coupled films has been investigated under this contract. Our results were all explainable on the basis that the island characteristics of thin copper layers cause free poles in the superimposed permalloy films; and, that the stray fields from these free poles increase the magnetization ripple structure. The situation concerning the role of free poles is quite similar to that of the columnar structure discussed above. We would expect a correlation between creep and ripple structure and would further expect that a discontinuous thickness in the intermediate film would lead to less domain-wall creeping. The latter conclusion has not been verified experimentally.

Since the main advantage of coupled films in ferromagnetic memory elements is expected to be diminished wall creeping, we have undertaken the study of wall creeping. As a result of these studies which appear in Appendix 2 we believe we have shown that Néel walls in coupled film can be stabilized against creeping.

The effect of combining uniaxial and biaxial anisotropy films has been investigated and it has been shown (Appendix 3) that such combinations may lead to favorable NDRO switching characteristics. Such a combination could readily be achieved through the utilization of coupled films.

In the device oriented studies of electro-deposited cylindrical coupled films we have shown that such elements can be prepared and that NDRO properties will be exhibited if suitable combinations of magnetic films and intermediate layers are utilized. We have shown that when the intermediate non-magnetic conducting layer is thin enough the film behaves as a unit and exhibits only one coercivity. Thicker intermediate layers provide stepped loops. We have investigated electroless Pd and electroless Cu as a means of providing the non-magnetic invervening coupling layer and have shown that electro-deposition is probably a more useful technique for obtaining the very thin films which are required. Due to our uncertainties about the continuity of the copper intervening layer we are unable to use these preliminary conclusions to achieve an understanding of the coupling mechanism. Pulse data on the films prepared so far have been inconclusive as regards their superiority from the creep standpoint in NDRO memory operations. Clearly further studies in cylindrical coupled film memory elements should be undertaken since the results obtained to date are encouraging.

REFERENCES

1. "Effect of Temperature and Environment on the Structure of Thin Single-Crystal Nickel Films," E. I. Alessandrini, J. Appl. Phys. 35, 1606 (1964).

2. "Influence of Minor Constituents in Ferromagnetic Films," R. J. Prosen, J. O. Holmen, B. E. Gran and T. J. Cebulla J. Phys. Soc. Japan 17, Suppl. B-I, 580 (1962).

3. "Influence of Minor Impurities in Ferromagnetic Films," R. J. Prosen, A. I. E. E. Great Lakes District Meeting, Minneapolis, Minnesota, April, 1961.

4. "A New Type of Magnetic Domain Structure in Negative Magnetostriction Ni-Fe Films," N. Saito, H. Fujiwara and Y. Sugita, J. Phys. Soc. Japan 19, 1116 (1964).

5. "Perpendicular Anisotropy Observed in Nickel and Nickel-Iron Magnetic Thin Films," S. Fujiwara, T. Koikeda and S. Chikazumi, J. Phys. Soc. Japan 20, 878 (1965).

6. "Anisotropie on magnetique superficielle et surstructures d'orientation", L. Neel, J. Phys. Radium 15, 225 (1954).

7. "New Magnetic Anisotropy," W. H. Meiklejohn and C. P. Bean, Phys. Rev. 105, 904 (1957).

8. "Columnar Structure in Thin Vacuum-Condensed Pd Films," R. H. Wade and J. Silcox, Appl. Phys. Letters 8, 7 (1966).

9. "Perpendicular Anisotropy of Ni and Fe Films," H. Fujiwara, Y. Sugita and N. Saito, J. Phys. Soc. Japan 20, 2088 (1965).

10. "Perpendicular Anisotropy in Nickel-Iron Magnetic Thin Films Evaporated at Low Substrate Temperature," T. Koikeda and S. Chikazumi, J. Phys. Soc. Japan 21, 399 (1966).

11. "An Estimation of Perpendicular Anisotropy of Magnetic Thin Films Originating from Non-Magnetic Grain Boundaries," H. Fujiwara, J. Phys. Soc. Japan 20, 2092 (1965).

12. "Wandbewegungsfeldstarken in magnetischen Mehrfachschichten," E. Feldtkeller, Z. Angew. Phys. 18, 532 (1965).

13. "The Effect of Alloy Composition on the Magnetization Ripple of Permalloy Films," A. Baltz, Proceedings of the International Conference on Magnetism, Nottingham (The Institute of Physics and the Physical Society, London, 1965), P. 845.

14. "Origin of Domain-Wall Creeping in Magnetic Films," A. Green, K. D. Leaver, and M. Prutton, J. Appl. Phys. 35, 812 (1964).

15. "Properties of Ni-Fe Double Films," S. Middelhoek, Z. Angew. Phys. 18, 524, (1965).

16. "A Mechanism of Magnetic Hysteresis in Heterogeneous Alloys," E. C. Stoner and E. P. Wohlfarth, Phil. Trans. Roy. Soc. London 240A, 599 (1948).

17. "Improved Magnetic Film Elements for Memory Application," E. Feldtkeller, K.. Stein, H. Harms, Intermag Proceedings, 1965, 8.4

18. J. C. Bruyere, et al. Intermag Proceedings, 1965, 5.1

19. "Switching Properties of Multilayer Thin Film Structure,"
A. Kolk, L. Douglas, G. Schrader, J. Appl. Phys. 33, 1061 (1962).

APPENDIX 1

PERPENDICULAR ANISOTROPY IN POLYCRYSTALLINE Ni-Fe THIN FILMS[1]

On the basis of the experiments initiated by the discovery of rotatable anisotropy[2], some of the present authors and their co-workers indicated[3] the importance of minor constituents and grain structure for the anomalous magnetic behavior of thin nickel-iron films. A film structure composed of columnar grains perpendicular to the film surface and separated by nonmagnetic grain boundaries (possibly oxide) was proposed. Saito, et al.,[4] showed that the rotatable anisotropy was attributable to the striped domain structure caused by the presence of a component of magnetic anisotropy with its easy axis perpendicular to the film surface. Saito, et al., tentatively attributed this anomalous component to the effect of internal stress. In the following, however, it will be shown that the perpendicular anisotropy can be explained by the magnetostatic energy of the discontinuous film structure mentioned above.

The structure of the film is simulated by an infinite two-dimensional array of ferromagnetic prisms with saturation magnetization I_s. The prisms (height L) have a square cross section (length of the sides D) and are arranged so that the side faces of any two prisms are parallel. The gap (distance d) between prisms is a nonmagnetic medium. The perpendicular anisotropy constant $K_\perp$ is defined by the energy expression

$$E = K_\perp \cos^2 \theta \tag{1}$$

where θ is the angle between magnetization and the normal to the film plane. Therefore, $K_\perp$ is given by

$$K_\perp = E_\perp - E_{||} \tag{2}$$

where $E_\perp$ and $E_{||}$ are the magnetostatic energies when the film is saturated perpendicular and parallel to the film plane, respectively. The value of $K_\perp$ should be $2\pi I_s^2$ for a uniform thin magnetic film. According to the sum theorem on generalized demagnetizing factors,[5] one can obtain the relation between $E_\perp$ and $E_{||}$ since any two orthogonal directions in the plane of the composite plate are equivalent. Therefore, $K_\perp$ is obtained by the straightforward calculation of the magnetostatic energy $E_\perp$. The surface density of free poles on the composite plate surface magnetized perpendicular to the plane is expressed by the double Fourier series

$$\omega = \pm \left(I_s \left[D/(D+d) \right]^2 + \omega' \right) \tag{3}$$

where plus and minus signs correspond to the two surfaces of the plate. The first term is independent of the coordinates in the plane of the plate. The second term ω' oscillates with these coordinates, the mean value of ω' is equal to zero. The magnetostatic energy due to the constant part of the surface density can be approximated by that of the very wide, thin ferromagnetic plate. The magnetostatic energy due to ω' is calculated by the standard Fourier series method.[6] Thus, the final expression for $K_\perp$ is as follows:

$$K_\perp = 2\pi I_s^2 \left(\frac{1}{2} \left(\frac{D}{D+d} \right)^2 \left[3 \left(\frac{D}{D+d} \right)^2 - 1 \right] + \frac{3D^2}{\pi^3 L (D+d)} \sum_{m=1}^{\infty} \frac{1}{m^3} \sin^2 \frac{m\pi D}{D+d} \left[1 - \exp\left(\frac{2m\pi L}{D+d} \right) \right] \right.$$

$$\left. + \frac{3(D+d)}{\pi^5 L} \sum_{m=1}^{\infty} \sum_{n=1}^{\infty} \frac{1}{m^2 n^2 (m^2+n^2)^{1/2}} \sin^2 \frac{m\pi D}{D+d} \sin^2 \frac{n\pi D}{D+d} \left\{ 1 - \exp \left[\frac{2\pi (m^2+n^2)^{1/2} L}{D+d} \right] \right\} \right) \tag{4}$$

In this expression, the contribution of the first term which came from the constant part in Eq. (3) for the surface density of free poles is much larger than the other terms. The results of the numerical calculation of $K_\perp$ are given in Fig. 1. It is apparent that $K_\perp (2\pi I_s^2)^{-1}$ depends strongly on d/D, but is almost independent of D/L.

In the above calculation the film was assumed to have flat surfaces. It can be shown, however, that the surface relief accompanying the columnar structure reduces the value of $K_\perp$ obtained above. An array of ferromagnetic prisms which have rounded (diameter c) end surfaces is considered. The surface density of free poles can be obtained for uniform magnetization perpendicular to the plate. For simplicity, the magnetostatic energy of this structure is substituted for that of the flat surface with the same surface distribution of free poles. Then, only the constant part of the surface density of free poles is taken into account, since the contribution of the periodic part is relatively small. Thus, the effective thickness d' of the grain boundary layer is approximately

$$d'/D = (d/D) + \frac{12}{5} \left(1 - \frac{1}{4}\pi\right)(c/D). \qquad (5)$$

Likewise, the uneven surface of a continuous film gives rise to perpendicular anisotropy which differs from $2\pi I_s^2$. However, the effect is small in comparison with the effect of surface relief accompanying the columnar structure.

In the case of the flat surface, one obtains $K_\perp (2\pi I_s^2)^{-1} \approx 0.84$ and 0.61 for the geometry L = 1000 Å, D = 300 Å, d = 10 Å, and L = 1000 Å, D = 300 Å, d = 30 Å, respectively. In the case of surface relief with c = 30 Å, the values $K_\perp (2\pi I_s^2)^{-1} \approx 0.66$ and 0.49 are obtained for the respective geometries.

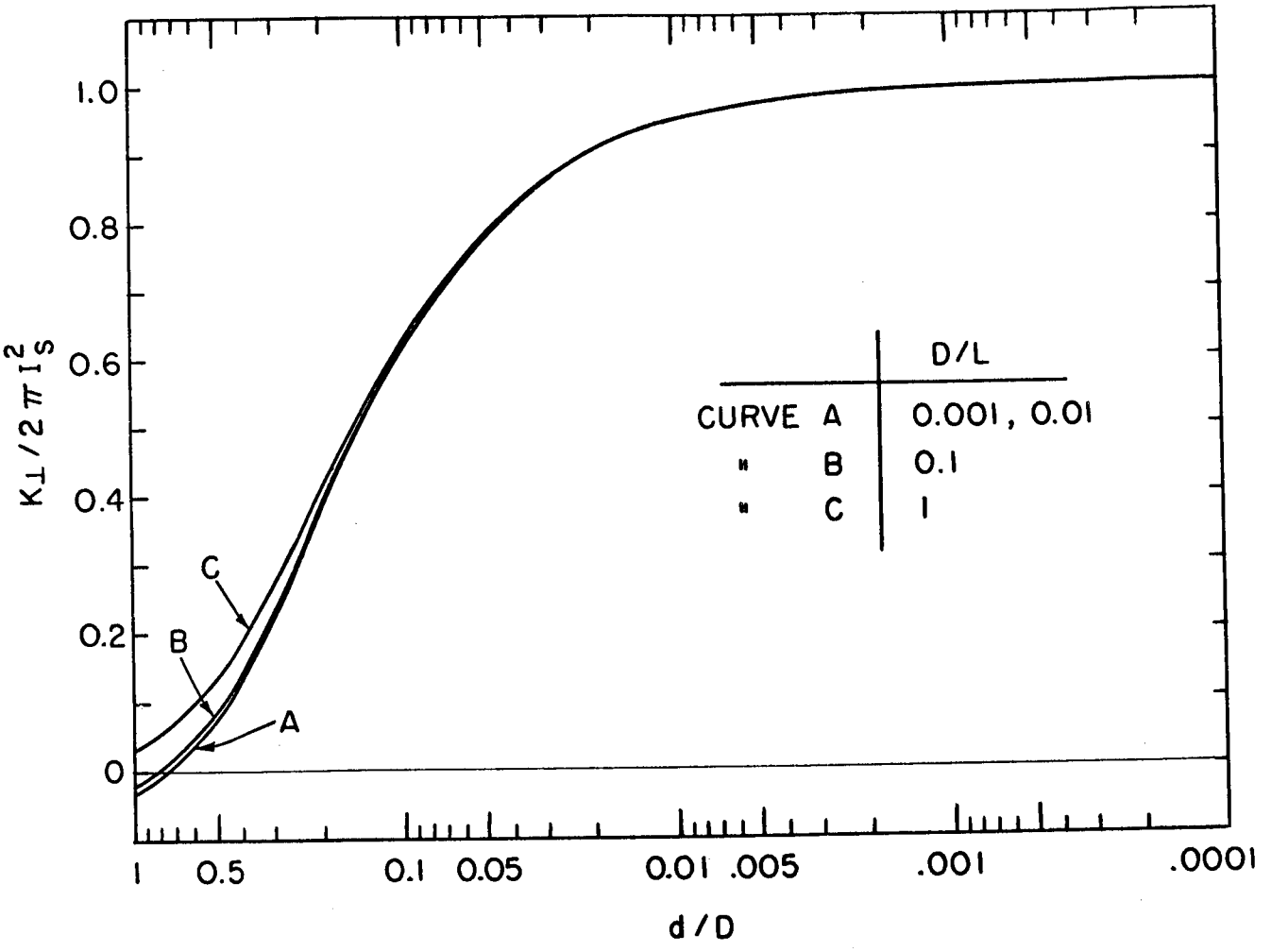

Figure 1 - CALCULATED PERPENDICULAR ANISOTROPY CONSTANT $K_\perp$ AS A FUNCTION OF THE FILM THICKNESS L, THE DIAMETER OF THE COLUMNAR GRAINS D, AND THE THICKNESS OF THE GRAIN BOUNDARY LAYER d.

Direct measurement by Fujiwara, et al.,[7] on Ni-Fe films of $K_\perp$ as a function of substrate temperature and composition shows $K_\perp \approx 2\pi I_s^2 \cdot f(T)$, where $f(T)$ is a function of substrate temperature and is equal to 0.8 and 0.5, respectively, for substrate temperatures 100° and 30° C. There may be a second-order dependence of $K_\perp$ upon magnetostriction according to the stress theory.[4] Our proposed calculation can explain the essential features of the experimental data utilizing previously published results that columnar grain structure is well developed[3] and that the columnar diameter is substrate temperature dependent (decreasing with decreasing substrate temperature)[8] if we make the assumption that the thickness of the grain boundary layer remains constant.

Our model also supports the experimental results that $K_\perp \approx 2\pi I_s^2$ [7, 9] for films deposited in very high vacuum since the impurity layer separating the columns is eliminated.

The measurement of the thickness dependence of the perpendicular anisotropy in 81% Ni-Fe polycrystalline films was made. Using a rotating shutter, films which have different thicknesses were deposited simultaneously onto glass substrates held at room temperature in a vacuum of 3×10^{-4} Torr. Figure 2 shows $K_\perp$ determined by torque measurement and the grain diameter obtained by electron microscopic observation. The perpendicular anisotropy constant calculated for the flat surface model is also given in the figure. The measured diameter of the grain was used and the thickness of the grain boundary layer was assumed to be constant (10 Å) for the calculation. The decrease of $K_\perp$ with decreasing thickness of the film agrees qualitatively with the prediction by the present model.

ACKNOWLEDGMENTS

The authors wish to thank Professor W. F. Brown, Jr., for valuable discussions and D. J. Sauve for the electron microscopic examinations.

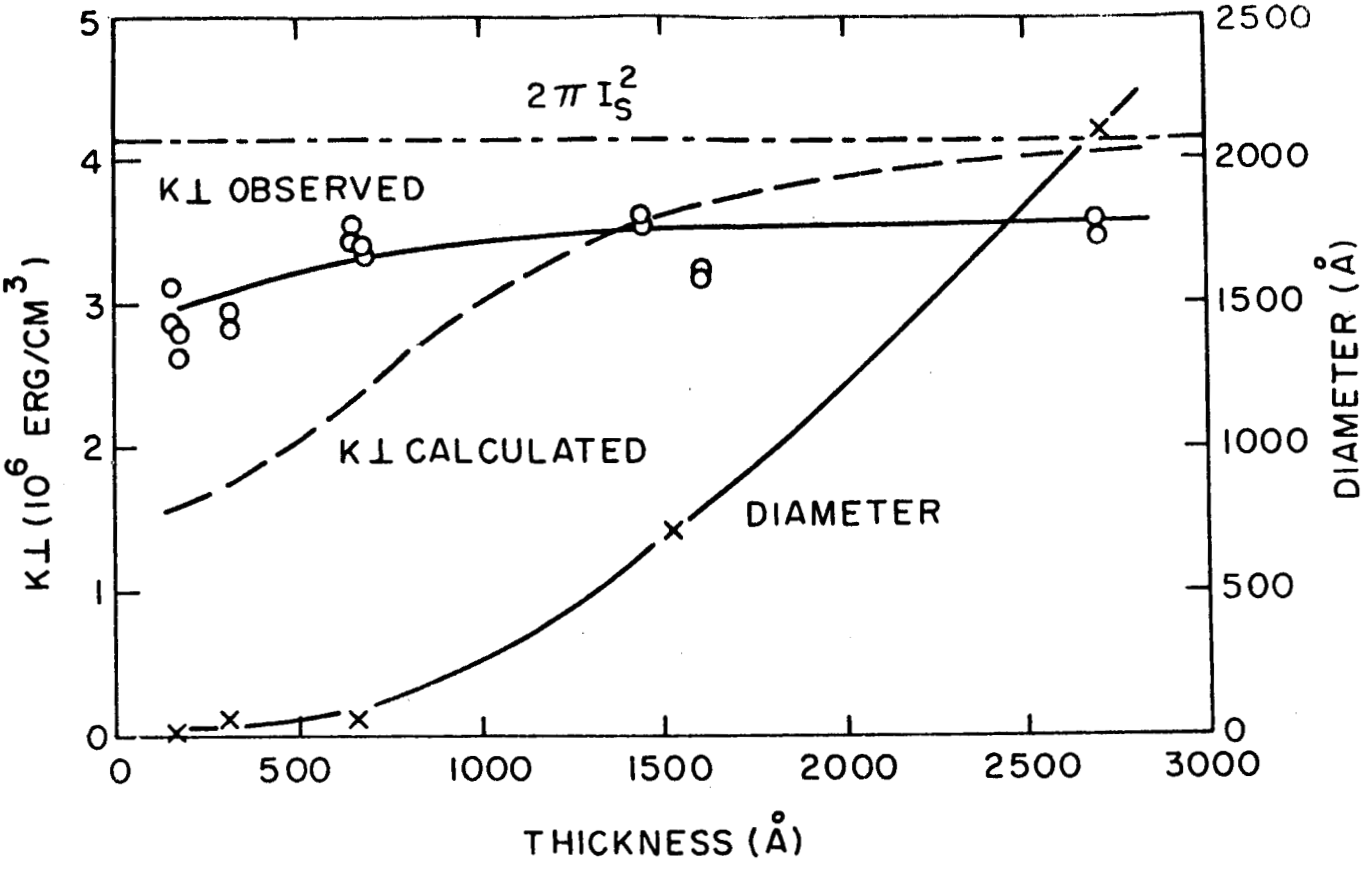

Figure 2 - OBSERVED AND CALCULATED PERPENDICULAR ANISOTROPY CONSTANTS $K_\perp$ AND THE DIAMETER OF GRAINS VERSUS THICKNESS OF THE FILM, FOR 81% Ni-Fe POLYCRYSTALLINE FILMS

REFERENCES

1. T. Iwata, R. J. Prosen, B. Gran, J. Appl. Phys. 37, 1285 (1966).

2. R. J. Prosen, J. O. Holmen, and B. E. Gran, J. Appl. Phys. 32, 91S (1961).

3. R. J. Prosen, J. O. Holmen, B. E. Gran, and T. J. Cebulla, J. Phys. Soc. Japan 17, Suppl. B-I, 580 (1962).

4. N. Saito, H. Fujiwara, and Y. Sugita, J. Phys. Soc. Japan 19, 1116 (1964).

5. W. F. Brown, Jr., Magnetostatic Principles in Ferromagnetism (North-Holland Publishing Company, Amsterdam, 1962), p. 51.

6. C. Kittel, Rev. Mod. Phys. 21, 541 (1949).

7. S. Fujiwara, T. Koikeda, and S. Chikazumi, J. Phys. Soc. Japan 20, 878 (1965).

8. M. H. Francombe, I. H. Khan, J. J. Flood, and M. M. Schlacter, in Single-Crystal Films, edited by M. H. Francombe and H. Sato (Pergamon Press, Inc., New York, 1964), p. 91.

9. J. F. Freedman, J. Appl. Phys. 36, 964 (1965).

APPENDIX 2
A MECHANISM FOR DOMAIN-WALL CREEPING IN MAGNETIC FILMS

A. INTRODUCTION

Domain-wall creeping may be observed when a dc field is applied to a magnetic film along an easy axis (longitudinal) and an ac field is applied along a hard axis (transverse). Even though the vectorial sum of the dc and ac fields lies well within the threshold curve which is obtained with longitudinal and transverse dc fields, the domain walls begin to move slowly so as to increase the volume of those domains magnetized parallel to the longitudinal dc field. Since this phomenon is important not only for a fundamental understanding of film properties but also for memory application, many studies have been made[1-8]. Several features of wall creeping have been displayed, remarkable among which are the strong dependences upon the types of walls[6, 7] and upon the conditions of applied transverse field[3, 6, 8]. On the origin of wall creeping, several mechanisms have been suggested[3-5, 8]. However, it is difficult at present to decide which of these theories is applicable. The purpose of this paper is to present an alternative mechanism for wall creeping.

B. EQUILIBRIUM STRUCTURE OF PARALLEL WALL SYSTEM

The model which will be considered is a system of parallel domain walls (P in Fig. 1) in an infinitely large film with uniaxial anisotropy. Uniform magnetization is assumed in individual domains A and B. The film thickness, mean separation of walls, and the wall thickness are denoted by T, W, and D, respectively.

An easy axis and the normal to the plane of the film are chosen respectively as the x and z axis of rectangular coordinates. In the absence of applied fields, the plane of an individual wall coincides with the (x z) plane. By the application of longitudinal and transverse dc fields $H_{||}$ and $H_{\perp}$, the

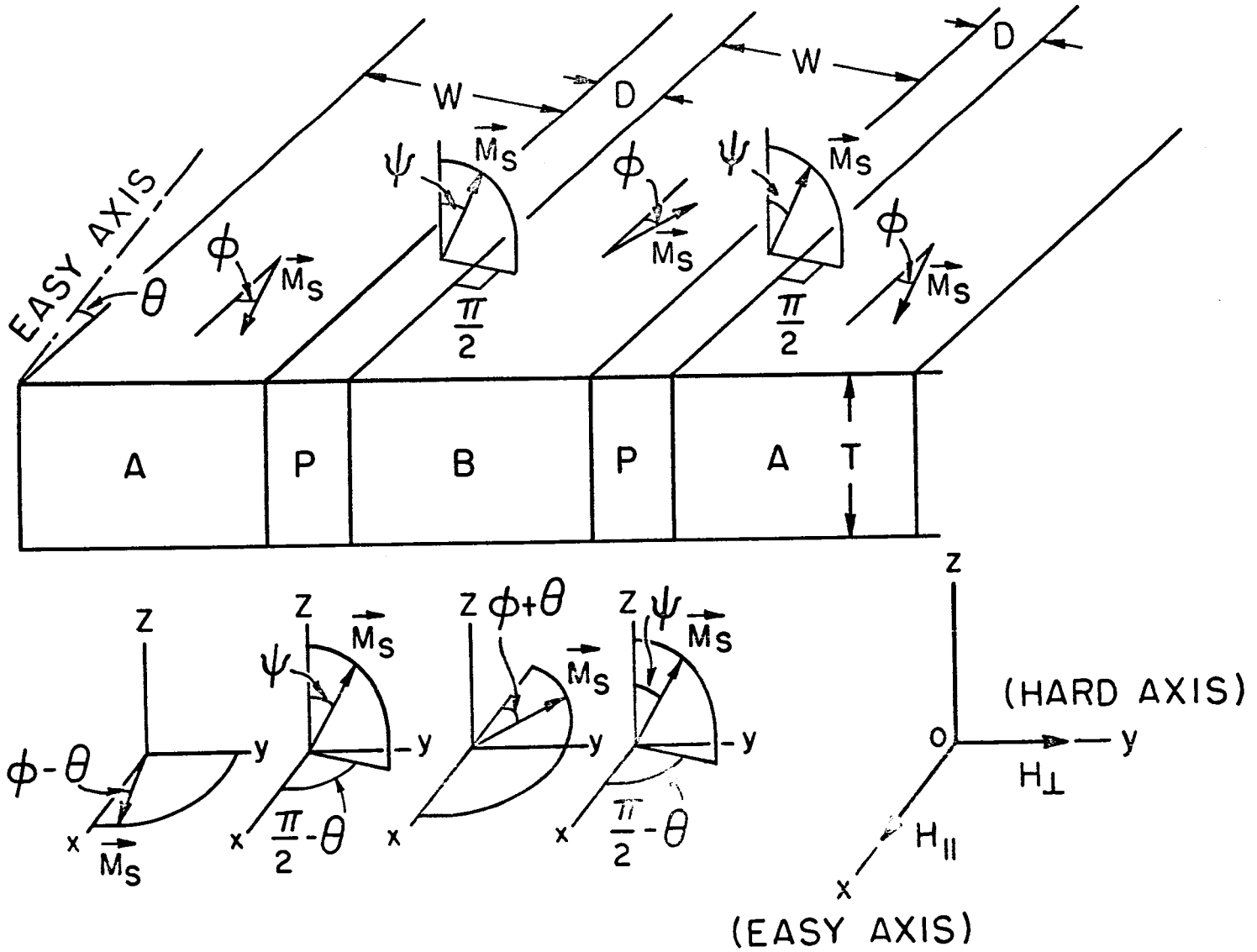

Figure 1 - A THIN FILM COMPOSED OF DOMAINS (A, B) SEPARATED BY PARALLEL WALLS (P) AND ASSOCIATED COORDINATES

magnetization vector in each domain rotates in the film plane. In general, rotation angles of magnetization vectors in neighboring domans, A and B in Fig. 1, are different and free poles will be induced at the wall separating them. In order to minimize the free-pole energy, the walls may rotate from their original position by an angle, θ, until the wall makes the same angle, φ, with the directions of magnetization in domains at both sides. Eventually the direction of magnetization in the domains A and B will make an angle $\varphi - \theta$ and $\varphi + \theta$ respectively with the easy axis. The direction of magnetization at the center of the wall is expressed by ψ and $\frac{1}{2}\pi - \theta$ as shown in the figure, so that in the case $\psi = 0$ or $\psi = \pm \frac{1}{2}\pi$ the wall is respectively of the Bloch type or the Néel type as found in the literature.

The ellipsoidal cylinder approximation[9] is used for the calculation of the magnetostatic energy of the wall. Since demagnetizing factors in the directions of the three major axes ∞, D, and T of the assumed cylinder are given respectively by 0, $4\pi T/(T+D)$, and $4\pi D/(T+D)$, the magnetostatic energy density of the wall which has effective magnetization $\underset{\sim}{M}$ (components in the three major axes being 0, M_D, and M_T) is approximated by $2\pi(TM_D^2 + DM_T^2)/(T+D)$. To find M_D and M_T, extremely thick and thin films are considered. The magnetostatic energy densities in these cases are approximated by $\pi M_s^2 (\sin\psi - \sin\varphi)^2$ and $\pi M_s^2 \cos^2\psi$, respectively, M_s being the saturation magnetization. By the comparison of these expressions in two extreme cases, M_D and M_T can be obtained separately, and it is assumed that these values hold irrespective of the film thickness. Thus the final expression of the magnetostatic energy density becomes $\pi M_s^2 [T(\sin\psi - \sin\varphi)^2 + D\cos^2\psi]/(T+D)$. The angle between the directions of magnetization in the domain and that at the center of the wall is $\cos^{-1}(\sin\varphi \sin\psi)$, so that the exchange energy density in the wall is approximated by $A[(2/D)\cos^{-1}(\sin\varphi \sin\psi)]^2$ in which A is the exchange constant. The possible optimum value of the ratio of the exchange

energy to the magnetostatic energy under weak applied fields, $\pi A M_s^{-2} D^{-3} (T+D)$, is, for example, roughly 0.6 in the case of the typical Permalloy film ($M_s = 8 \times 10^2$ G, $A = 10^{-6}$ erg/cm, $T = 1000$ Å, and $D = 500$ Å). Then the exchange energy is neglected for the sake of simplicity. It can be shown that this will give no essential change in the result. The anisotropy energy term in the wall energy can be safely neglected. Thus the total energy referred to the unit volume of the whole system is given by

$$E = -\frac{1}{2}\left\{ K\left[\cos^2(\varphi-\theta)+\cos^2(\varphi+\theta)\right] + M_s H_{\parallel}\left[\cos(\varphi-\theta)-\cos(\varphi+\theta)\right] + M_s H_{\perp}\left[\sin(\varphi-\theta)+\sin(\varphi+\theta)\right]\right\} + \frac{\pi M_s^2 D}{W(T+D)}\left[T(\sin\varphi-\sin\psi)^2 + D\cos^2\psi\right], \quad (1)$$

where K is the uniaxial anisotropy constant and $W >> D$ is assumed.

Assuming that W and D are both constant, the energy expression is minimized with respect to θ, φ, and ψ. Corresponding to the conditions that $T/D \gtrless 1 + \pi M_s^2 D(2KW)^{-1}$, the Bloch walls ($\psi = 0$) or the Néel walls ($\psi = \pm\frac{1}{2}\pi$) are found to be stable in the absence of applied fields. For $h_{\parallel} = H_{\parallel}/H_k << 1$ and $h_{\perp} = H_{\perp}/H_k << 1$ ($H_k = 2K/M_s$), the following solutions are obtained.

1) System of parallel Bloch walls

$$\theta = \frac{h_{\parallel} h_{\perp}}{1-R}, \qquad \varphi = \frac{h_{\perp}}{1-R}, \qquad \text{and } \psi = \frac{T h_{\perp}}{(1-R)(T-D)}$$

$$\text{with } R = \frac{\pi M_s^2 T D^2}{KW(T^2-D^2)}. \quad (2)$$

ii) System of parallel Néel walls

$$\left.\begin{aligned} \theta &= \frac{h_{\parallel} \sin\varphi}{1-2\sin^2\varphi + h_{\perp}\sin\varphi} \qquad \text{and } \sin\varphi = \frac{\pm S + h_{\perp}}{1+S} \\ \text{with } S &= \frac{\pi M_s^2 \, TD}{KW\,(T+D)} , \end{aligned}\right\} \tag{3}$$

where the ± signs are associated with $\psi = \frac{1}{2}\pi$ or $\psi = -\frac{1}{2}\pi$.

According to Eq. (3), even when the applied field is absent, the angle φ in the case of the Néel wall system has a finite value, i. e., the directions of magnetization in the domains separated by the Néel wall deviate from the easy axis and cant with one another. Assuming $M_s = 8 \times 10^2$ G, $K = 10^3$ erg/cm^3, $T = 500$Å, $W = 10^{-2}$cm, and $D = 500$Å, one obtains $|\varphi| \approx 20°$. The cause of the canting is the large magnetostatic energy inherent in the Néel wall. A somewhat similar case was qualitatively discussed and observed experimentally by Feldkeller[10]. Peculiar creep properties of Néel walls are attributed to this phenomenon.

C. WALL MOTION THRESHOLDS

We now proceed to calculate the wall motion threshold fields. The threshold field is determined by the condition that the pressure induced on the wall by the application of magnetic fields is just counterbalanced by the maximum value of the restoring force (i. e., the maximum value of the spatial variation of effective wall energy $(\partial \epsilon / \partial s)_{max}$). Thus, one finds

$$M_s H_{\parallel} [\cos(\varphi-\theta) + \cos(\varphi+\theta)] + M_s H_{\perp} [\sin(\varphi-\theta) - \sin(\varphi+\theta)]$$

$$+K [\cos^2(\varphi-\theta) - \cos^2(\varphi+\theta)] = \left(\frac{\partial \epsilon}{\partial s}\right)_{max}. \qquad (4)$$

The last term in the left hand side of the equation is an additional pressure due to the fact that the deviation of the magnetization from the easy axis is different in domains at opposite sides of the wall. At present, there are diverse arguments about the origin of wall coercivity, or $(\partial \epsilon / \partial s)_{max}$, which operates in thin films[11]. Here, it is simply assumed that $(\partial \epsilon / \partial s)_{max}$ is independent of applied magnetic fields. By the substitution of Eq. (2) or (3) into Eq. (4), the following equations for wall motion threshold curves are obtained.

i) System of parallel Bloch walls

$$\left.\begin{aligned} (h_{\parallel})_c &= (h_{\parallel})_{co} [1 + (h_{\perp})_c^2 \cdot F(R)] \\ \text{with } (h_{\parallel})_{co} &= \frac{1}{4K} \left(\frac{\partial \epsilon}{\partial s}\right)_{max.} \end{aligned}\right\} \qquad (5)$$

ii) System of parallel Néel walls

$$\left.\begin{aligned} (h_{\parallel})_c &= (h_{\parallel})_{co} [1 \pm (h_{\perp})_c \cdot G_1(S) + (h_{\perp})_c^2 \cdot G_2(S)] \\ \text{with } (h_{\parallel})_{co} &= \frac{1}{4K} \left(\frac{\partial \epsilon}{\partial s}\right)_{max} \cdot \alpha(S), \end{aligned}\right\} \qquad (6)$$

where the ± signs are associated with $\psi = \frac{1}{2}\pi$ or $\psi = -\frac{1}{2}\pi$. Here, $(h_{\parallel})_{co}$ is the threshold field along the easy axis when $h_{\perp} = 0$ or the wall coercivity, and the small values of $(h_{\parallel})_c$, $(h_{\perp})_c$, and $(h_{\parallel})_{co}$ are assumed for the calculation. Explicit expressions for $F(R)$, $G_1(S)$, $G_2(S)$, and $\alpha(S)$ are given in the conclusion of this appendix. Wall motion threshold curves calculated using values for typical Permalloy films are shown in Figs. 2 and 3.

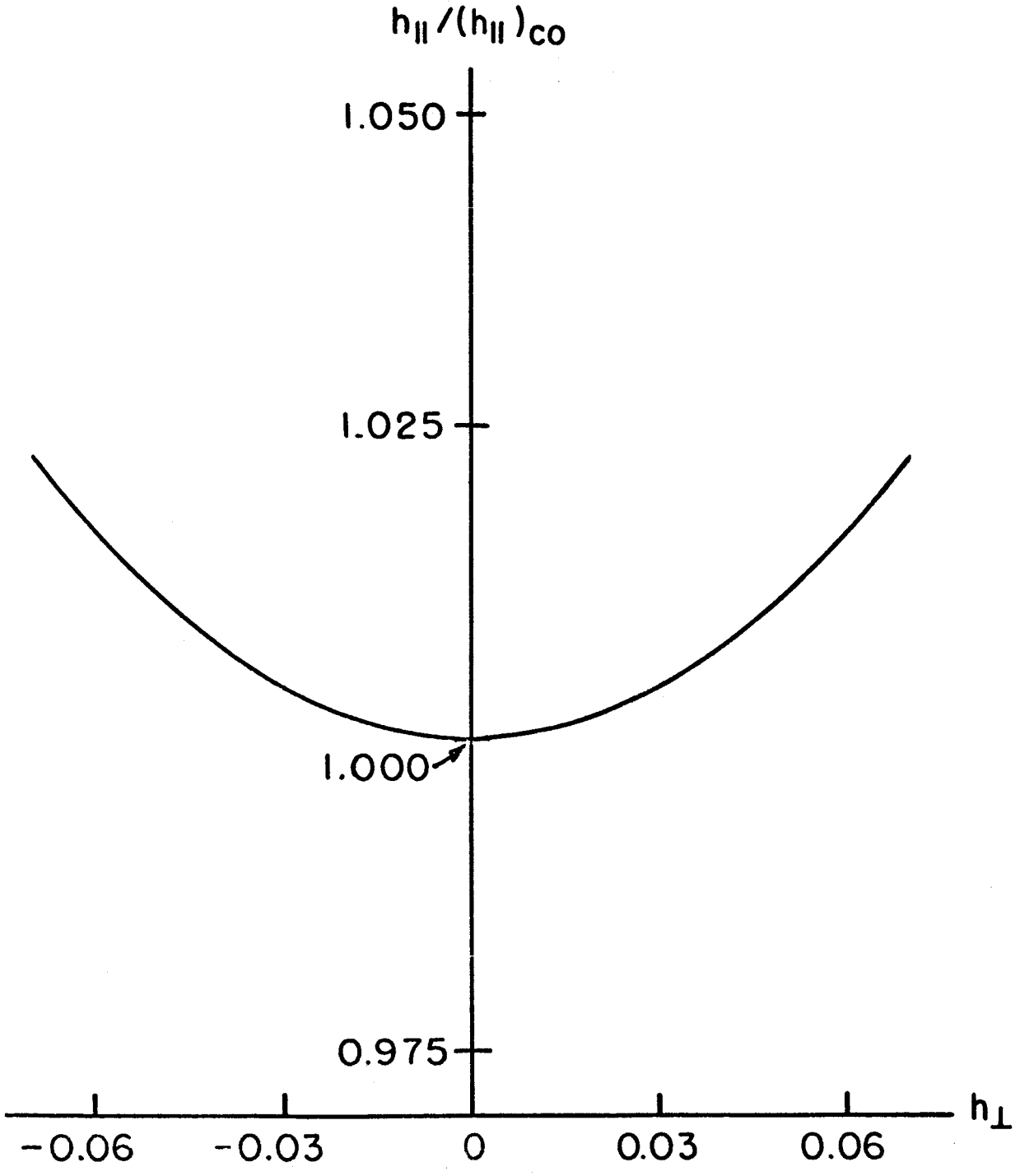

Figure 2 - THRESHOLD CURVE FOR THE MOTION OF BLOCH WALLS [$M_s = 8 \times 10^2$G, $K = 10^3$ erg/cm^3, T = 1000Å, $W = 10^{-2}$ cm, AND D = 500Å].

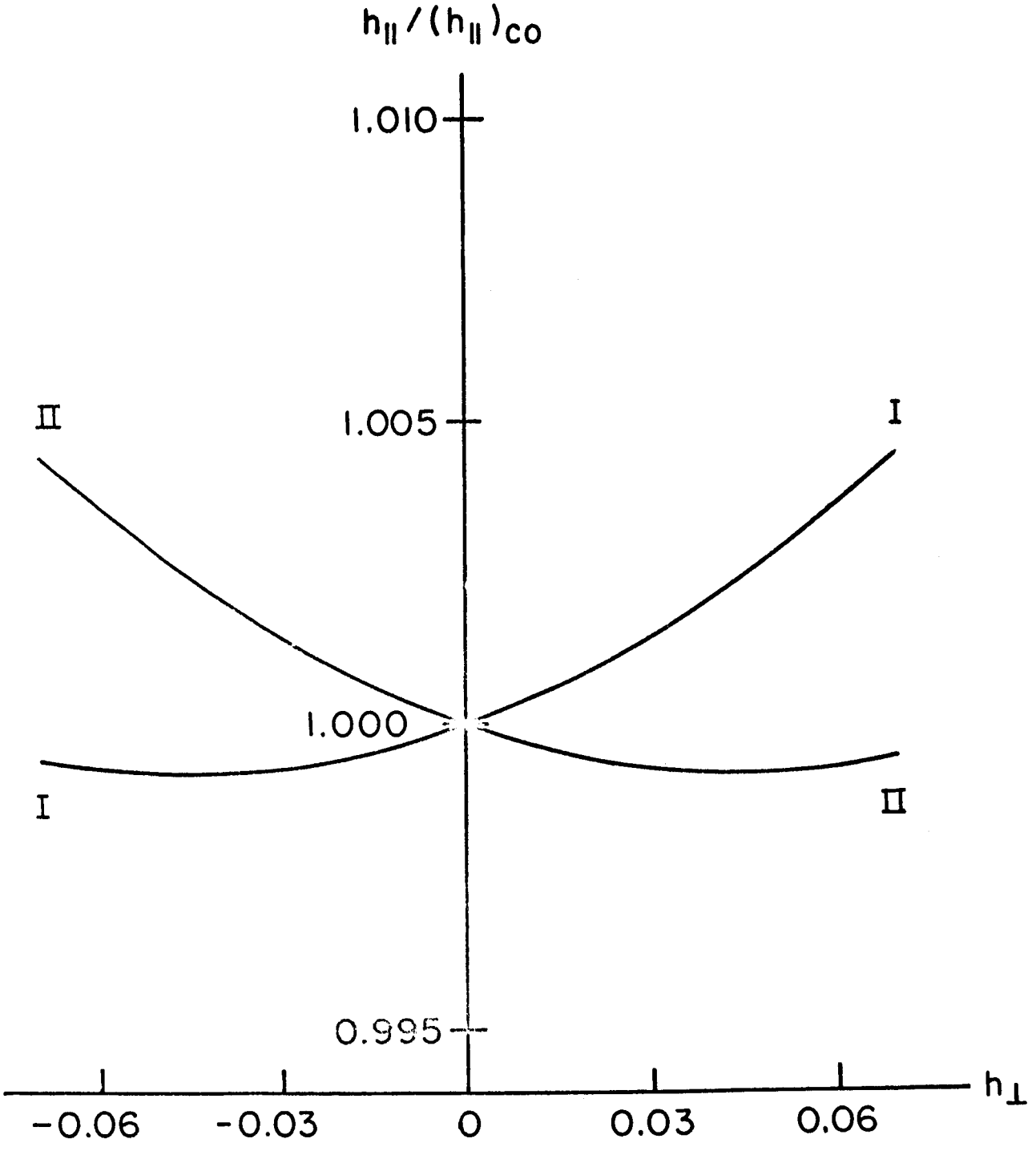

Figure 3 - THRESHOLD CURVES FOR THE MOTION OF NÉEL WALLS, I FOR THE WALLS WITH $\psi = \frac{1}{2}\pi$ and II for those with $\psi = -\frac{1}{2}\pi$ [$M_s = 8 \times 10^2$G, $K = 10^3$ erg/cm^3, $T = 500\text{Å}$, $W = 10^{-2}$ cm, and $D = 500\text{Å}$].

The threshold curve for the Bloch wall motion (Fig. 2) is concave downwards. Corresponding to the Néel wall with $\psi = \frac{1}{2}\pi$ or $\psi = -\frac{1}{2}\pi$, two threshold curves I or II in Fig. 3 are obtained. Each curve is the mirror image of the other and asymmetric with respect to the ordinate.

The Néel wall which actually occurs may be the composition of wall segments with $\psi = \frac{1}{2}\pi$ and $\psi = -\frac{1}{2}\pi$ separated by Bloch lines as in the cross-tie wall. This composite structure is adopted for the model of the actual Néel wall or the cross-tie wall (the contribution from the cross-ties is neglected), and it is assumed that the walls are originally composed of the same amounts of components and that the unbalance between segments with $\psi = \frac{1}{2}\pi$ and with $\psi = -\frac{1}{2}\pi$ occurs irreversibly by the movement of Bloch lines when the intensity of the transverse field becomes equal to the Bloch-line coercivity, h_c. Now consider the threshold field along the easy axis when the transverse field is changed in the following two ways.

i) The transverse dc field is changed to a given value starting from zero, and then the threshold field along the easy axis is measured. If the magnitude of the transverse dc field is smaller than the Bloch-line coercivity h_c, the two kinds of segments are equal in their amounts. The corresponding threshold curve is the mean curve of Curves I and II in Fig. 3; the threshold curve segment p_0p_1 (or p_0p_{-1}) in Fig. 4(a) is obtained. If the transverse dc field is larger than h_c, wall segments with $\psi = \frac{1}{2}\pi$ predominate over the other component. The corresponding threshold curve is Curve I in Fig. 3, * the threshold curve segment p_2p_3 in Fig. 4(a) being obtained. A similar argument is applied for negative values of the transverse field, $p_{-2}p_{-3}$ being obtained. Eventually the whole threshold curve for this case is as shown in Fig. 4(a).

---

* Strictly speaking, here and in the following, the true threshold curves are slightly different from the curves given in Fig. 3, because the walls being discussed contain the small amount of unfavorable segments. However, this discrimination is not important and then is omitted in the present qualitative discussions.

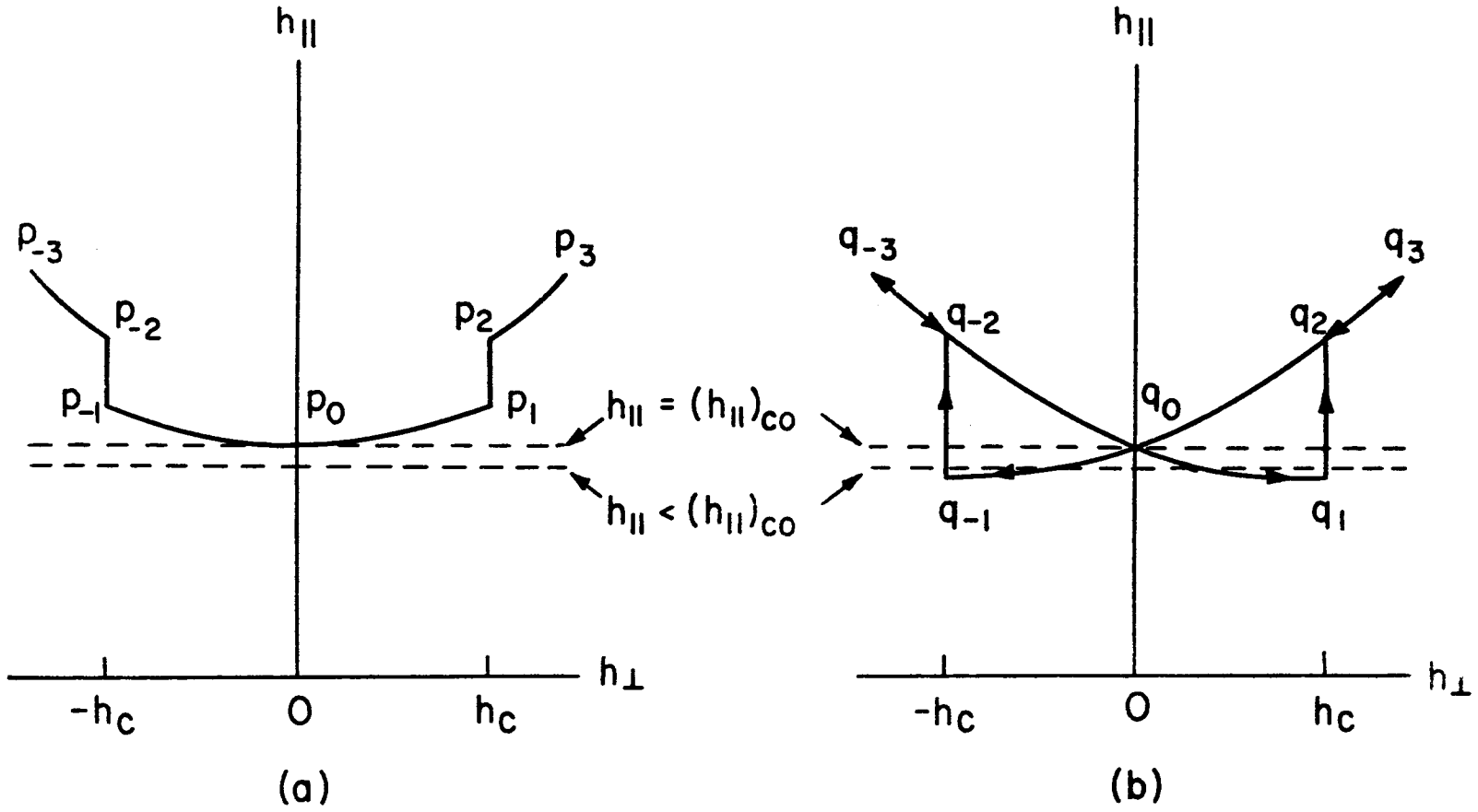

Figure 4 - HYPOTHETICAL THRESHOLD CURVES FOR THE MOTION OF NÉEL WALLS COMPOSED OF SEGMENTS WITH $\psi = \frac{1}{2}\pi$ and $\psi = -\frac{1}{2}\pi$. (a) FOR TRANSVERSE dc FIELD, (b) FOR TRANSVERSE ac FIELD. DASHED LINES ARE THE LOCI OF THE VECTORIAL SUM OF THE APPLIED FIELDS, AND h_c IS THE BLOCH-LINE COERCIVITY.

ii) After the transverse field was changed alternatively between plus and minus maximum values, of which the magnitude is larger than h_c, the threshold field along the easy axis is measured at some value of the transverse field. The Bloch-line motion is assumed to be irreversible and the $\psi = -\frac{1}{2}\pi \longrightarrow \frac{1}{2}\pi$ or $\psi = \frac{1}{2}\pi \longrightarrow -\frac{1}{2}\pi$ transformation occurs respectively at $h_\perp = h_c$ or $h_\perp = -h_c$. Therefore, in the ranges $h_\perp > h_c$ with increasing $h_\perp$ and $h_\perp > -h_c$ with decreasing $h_\perp$, $\psi = \frac{1}{2}\pi$ segments predominate over the other component in individual walls and Threshold Curve I in Fig. 3 is applied. In the ranges $h_\perp < -h_c$ with decreasing $h_\perp$ and $h_\perp < h_c$ with increasing $h_\perp$, $\psi = -\frac{1}{2}\pi$ segments predominate and Threshold Curve II in Fig. 3 is applied. Thus, eventually, the threshold curve $q_0\, q_1\, q_2\, q_3\, q_2\, q_0\, q_{-1}\, q_{-2}\, q_{-3}\, q_{-2}\, q_0 \ldots$ in Fig. 4(b) is obtained for this case.

D. DISCUSSIONS

Now, let us discuss the movement of walls when a dc field, $h_{\parallel} \leqq (h_{\parallel})_{co}$, is applied along the easy axis and an ac field, of which the amplitude is larger than h_c, is applied along the hard axis as in the standard creep experiment. In the case of Bloch walls, owing to the concavity downwards of the threshold curve (Fig. 2), the vectorial sum of the dc and ac fields is always within the threshold curve. Therefore, at least so long as the amplitude of the transverse ac field remains small, the Bloch walls do not creep. In the case of composite Néel walls, the situation is quite different. During each cycle of the transverse ac field with the constant longitudinal field, $h_{\parallel} = (h_{\parallel})_{co}$, twice, in the range $0 < h_\perp < h_c$ with increasing $h_\perp$ and in the range $-h_c < h_\perp < 0$ with decreasing $h_\perp$, the threshold curve (Fig. 4(b)) falls beneath the locus of the vectorial sum of the applied fields and therefore walls are brough into movement. For $h_{\parallel} < (h_{\parallel})_{co}$, so long as the locus intersects the threshold curve, wall creeping occurs. In all of these cases, the vectorial sum of the applied fields is surely well within the threshold curve associated with longitudinal and transverse

dc fields (Fig. 4 (a)). The thinner films in which cross-tie walls occur show large amounts of wall creeping, and, in contrast to this, wall creeping in thicker films in which walls are mostly of Bloch type is depressed so long as the transverse ac field is small [6, 7] . These experimental results are well predicted by the above considerations.

When a constant ac field is biased by a dc field in the transverse direction and the strength of the latter becomes larger, creeping of cross-tie walls is suppressed remarkably[6] . It was also found experimentally[3] that the creep of Néel walls did not occur if the transverse pulse fields superimposed on the longitudinal dc field were all in the same direction, nevertheless creep could be induced by superimposing the transverse pulse field alternatively in one direction and then the other. These results are understood as follows. By the application of a large enough bias field or uni-directional pulse fields, in each Néel wall the segments in which the direction of effective magnetization is parallel to the bias field or the pulse fields predominate over the segments of the opposite kind. The corresponding threshold curve is $q_0\, q_3$ (or $q_0\, q_{-3}$) in Fig. 4(b), wall creeping being prevented. In order to maintain the same amount of creeping when the transverse dc bias field is increased from zero to some value, the resultant of the transverse ac and dc fields, $h_\perp$, should cover the whole range of $-h_c \leqq h_\perp \leqq h_c$ in Fig. 4(b); the amplitude of the transverse ac field is to be increased by an amount equal to the applied transverse dc bias field. Thus the critical amplitude of a transverse ac field vs. longitudinal dc field curve is expected to be displaced along the transverse field direction by an amount equal to a transverse dc bias field. This may be an alternative explanation of the displacement of the threshold curve observed on the 875Å - thick Permalloy film[8] in which cross-tie walls appear[7].

On the role of the Bloch-line motion, the following should be indicated. Experimentally, it was observed[1, 2, 6] that domain-wall creeping was associated with Bloch-line motion. Some theory[5] attributed the cause of wall creeping to the motion of Bloch lines. In the present model, the Bloch-line motion does occur during wall creeping. However, the wall creeping is interrupted after the occurrence of the Bloch-line motion in each half cycle of the transverse ac field.

In the calculation of the threshold curve, it has been assumed that $(\partial \epsilon / \partial s)_{max}$ is independent of applied fields. By an analysis of the available experimental data, it is observed that this is not always the case. If so, the wall motion threshold curves derived above should be modified. However, this will not change the essential features of the present results such as the comparison of creep properties of the walls of different types or the comparison under different conditions of the transverse field.

E. CONCLUSION

Summarizing, although the calculation has been made on an over simplified model and only in the range of weak longitudinal and transverse fields, one can say that the main features of the wall creeping are understood on the basis of the present theory. Wall creeping during Bloch-Néel wall type transitions will be the subject of further study.

EXPRESSIONS

Explicit expressions for $F(R)$, $G_1(S)$, $G_2(S)$ and $\alpha(S)$ are as follows:

$$F(R) = \frac{1}{2(1-R)^2} ,$$

$$G_1(S) = \frac{S^2(1-S)}{(1+2S)\left[(1+S)^2 - 2S^2\right]} ,$$

$$G_2(S) = \frac{1}{1+2S}\left\{S + \frac{(1+S)^2 + 2S^2(1-S)}{2(1+2S)} - \frac{S^2(1-S)(4-S)}{(1+S)^2 - 2S^2}\right.$$

$$\left. - \frac{S^4(3-S)^2}{\left[(1+S)^2 - 2S^2\right]^2} + \frac{S^4(3-S)}{(1+2S)\left[(1+S)^2 - 2S^2\right]} + \frac{S^4(1-S)^2}{(1+2S)\left[(1+S)^2 - 2S^2\right]^2}\right\},$$

and $$\alpha(S) = \frac{(1+S)\left[(1+S)^2 - 2S^2\right]}{(1+2S)^{3/2}} .$$

REFERENCES

1. S. Middelhoek, Z. Angew. Phys. 14, 191 (1962).

2. E. Fuchs and H. Pfisterer, Proceedings of the 5th International Congress for Electron Microscopy (Academic Press, Inc., New York, 1962), II-4.

3. T. H. Beeforth and P. U. Hulyer, Nature 199, 793 (1963).

4. A. Green, K. D. Leaver, and M. Prutton, J. Appl. Phys. 35, 812 (1964).

5. A. Green, K. D. Leaver, R. M. Livesay, and M. Prutton, Proceedings of the International Conference on Magnetism, Nottingham, 1964 (The Institute of Physics and the Physical Society, London, 1965), p. 807.

6. S. Middelhoek, Phys. Letters 13, 14 (1964).

7. A. L. Olson and E. J. Torok, J. Appl. Phys. 36, 1058 (1965).

8. A. L. Olson and E. J. Torok, J. Appl. Phys. 37, 1297 (1966).

9. See, e.g., R. F. Soohoo, Magnetic Thin Films (Harper and Row Publishers, New York, 1965), p. 40.

10. E. Feldtkeller, Z. Angew. Phys. 13, 161 (1961).

11. See, e.g., R. F. Soohoo, op. cit., p. 141.

APPENDIX 3

SWITCHING CHARACTERISTICS OF UNIAXIAL FERROMAGNETIC THIN FILMS WITH SUPERIMPOSED BIAXIAL ANISOTROPY

The requirements for film characteristics in nondestructive readout, NDRO, with uniaxial bits may be a large output signal and a small digit field for the specified value of the drive field (for example 80% of the hard axis saturation field). These can be satisfied in films which have a switching curve elongated in the hard axis and accompanied by a hard-axis magnetization curve with upward concavity. This appendix reports a way to meet these requirements by controlling film anisotropies.

Consider a thin film which has uniaxial and superimposed biaxial anisotropies and is subjected to fields both in the easy axis and in the hard axis ($H_{\parallel}$ and $H_{\perp}$). The energy expression is given by

$$E = K_u \sin^2 \varphi + K_b \sin^2 \varphi \cos^2 \varphi - M_s H_{\parallel} \cos \varphi - M_s H_{\perp} \sin \varphi, \qquad (1)$$

where K_u (> 0) and K_b are respectively the uniaxial and the biaxial anisotropy constant, φ is the angle of the magnetization vector measured from the easy axis of uniaxial anisotropy, and M_s is the saturation magnetization. By putting $\partial E/\partial \varphi = \partial^2 E/\partial \varphi = 0$, parametric equations for the threshold curve for coherent-rotational switching are obtained as follows:

$$\left.\begin{aligned} (H_{\parallel})_c &= -\frac{2K_u}{M_s} \cos^3 \varphi [1 - \alpha(5 - 6\cos^2 \varphi)], \\ (H_{\perp})_c &= \frac{2K_u}{M_s} \sin^3 \varphi [1 + \alpha(5 - 6\sin^2 \varphi)] \end{aligned}\right\} \qquad (2)$$

$$\text{with } \alpha = \frac{K_b}{K_u} .$$

This expression was first derived by Pugh,[1] and discussions were made on the switching of biaxial films with or without modification by uniaxial anisotropy in the range $1 \leq \alpha \leq \infty$. In the following, attention will be focused on the range $-1 \leq \alpha \leq 0$, so that the films have a single resultant easy axis in the direction $\varphi = 0$ (easy axes of the biaxial anisotropy are in the directions $\varphi = \pm \pi/4$).

Calculated switching threshold curves are given in Figure 1. When the value of α decreases from zero, starting from the original Stoner-Wohlfarth asteroid ($\alpha = 0$), the switching curve elongates in the hard axis with large modifications in its shape in the neighborhood of the easy axis. The portion given by the dashed line is not important because it is associated with the high energy state during coherent rotation. Thus, the flat switching curves drawn by the full line are realized. Magnetization curves are calculated using the equation $\partial E/\partial \varphi = 0$. The easy axis magnetization loops ($M_{||}$ vs $H_{||}$ with $H_{\perp} = 0$) and hard axis magnetization curves ($M_{\perp}$ vs $H_{\perp}$ with $H_{||} = 0$) are given respectively in Figure 2 (a) and (b). The hard axis magnetization curves for $\alpha < 0$ are concave upward in fields of less than the saturation field, in contrast to the straight line for $\alpha = 0$. Therefore, for any fixed value of the ratio (R) of the applied hard axis field to the hard axis saturation field, the relative magnetization $M_{\perp}/M_s$ for $\alpha < 0$ is larger than that for $\alpha = 0$ (when the comparison is made, e.g., at $R = 0.80$, $M_{\perp}/M_s = 0.80$ for $\alpha = 0$ and $M_{\perp}/M_s = 0.93$ for $\alpha = -1.0$). This means that the larger read out signal is obtained for the film with a smaller value of α. Thus it can be said that a uniaxial film modified by biaxial anisotropy is favorable in NDRO memory application.

On the fabrication of the film discussed above, the following should be mentioned. In order to obtain uniaxial anisotropy, conventional techniques such as deposition or annealing in an orienting field can be used. For obtaining biaxial anisotropy, the single crystal film technique[1] or the periodic surface relief technique[2] may be utilized. It does not matter whether the two anisotropies are carried together in a single film or separately in two layers in a coupled film.

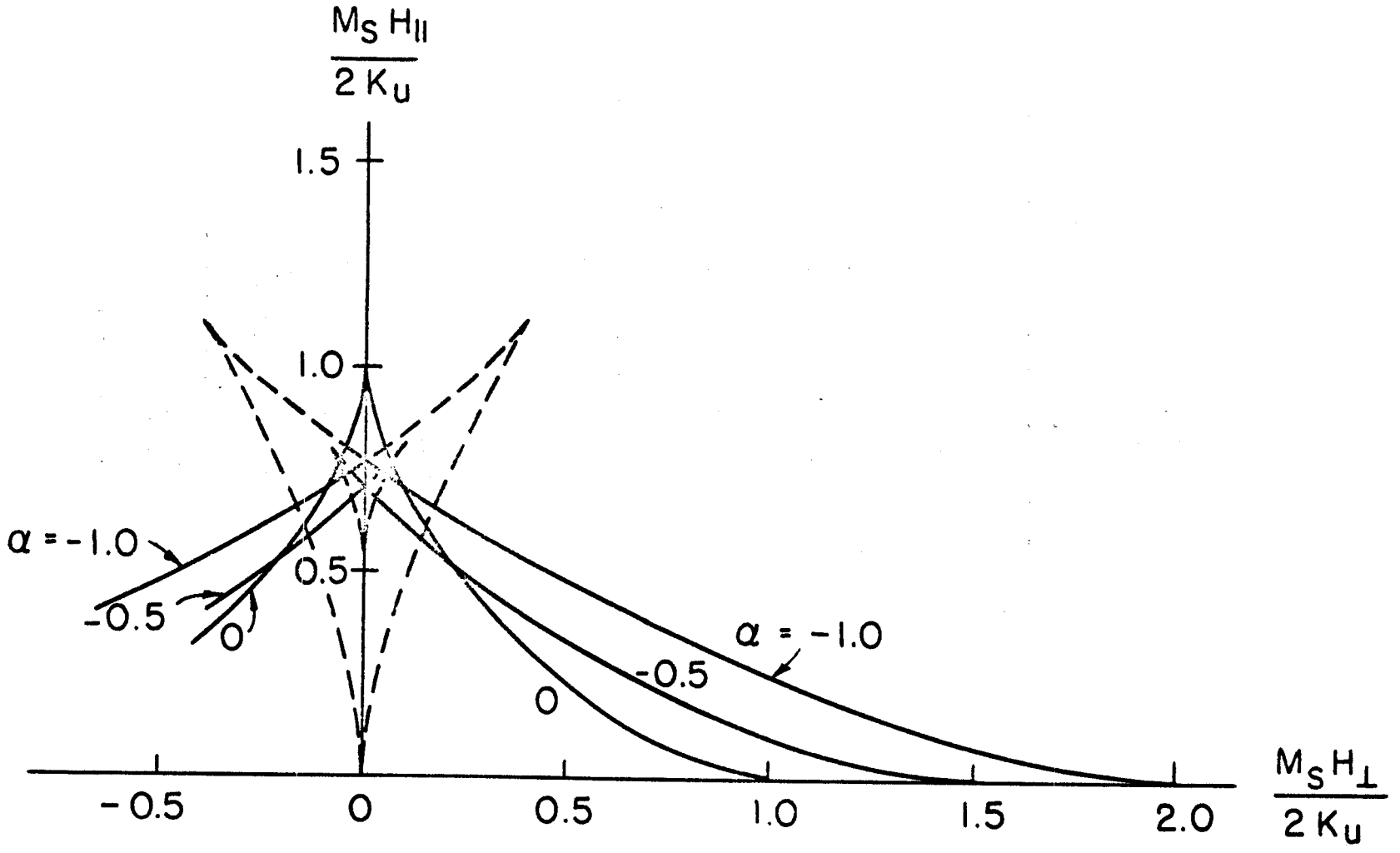

Figure 1 - SWITCHING CURVES FOR COHERENT ROTATION ($\alpha = K_b/K_u$). DASHED LINE CURVES ARE NOT REALIZED ENERGETICALLY.

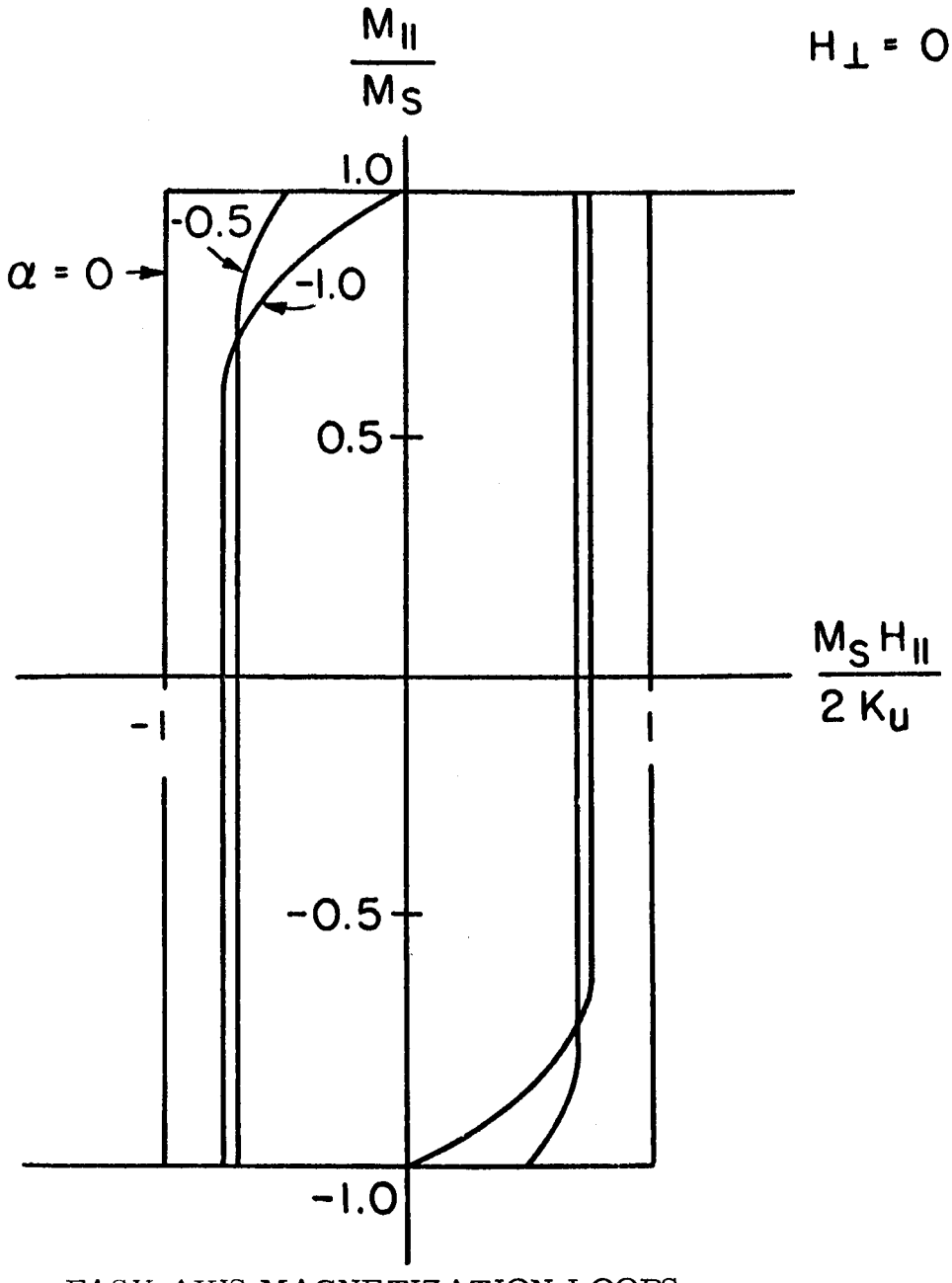

Figure 2(a) - EASY-AXIS MAGNETIZATION LOOPS

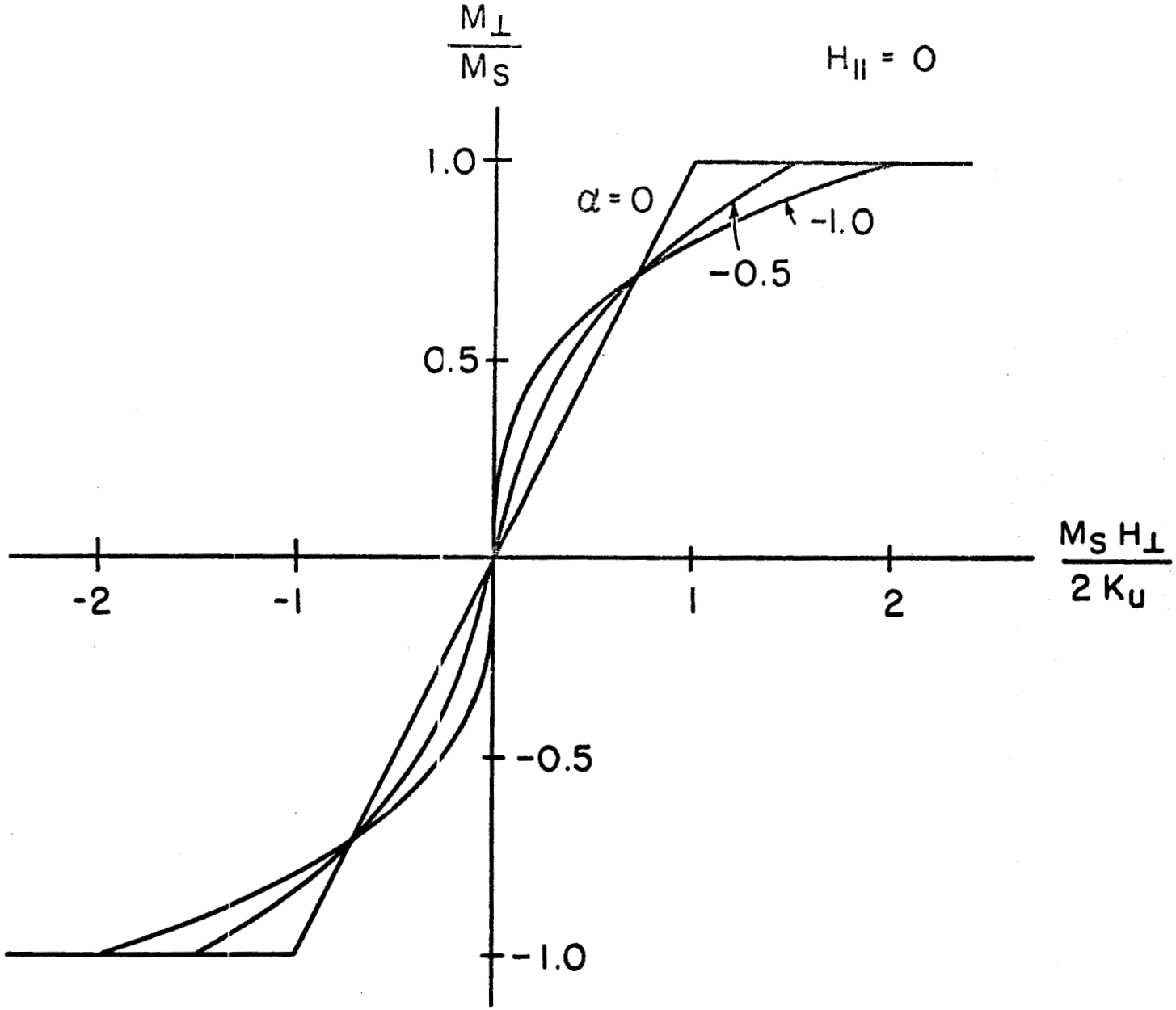

Figure 2(b) - HARD-AXIS MAGNETIZATION CURVES ($\alpha = K_b/K_u$).

REFERENCES

1. E. W. Pugh, Proc. Intermag Conf., 1963, p. 15 -1-1: A. Yelon, O. Voegeli, and E. W. Pugh, J. Appl. Phys. 36, 101 (1965).

2. R. J. Prosen, Y. Gondo and B. E. Gran, J. Appl. Phys. 35, 826 (1964): Y. Gondo, B. E. Gran, and R. J. Prosen, J. Appl. Phys. 36, 1062 (1965).